

Deep low-frequency observations with the Giant Metrewave Radio Telescope: a search for relic radio emission

S. K. Sirothia,^{*} D. J. Saikia, C. H. Ishwara-Chandra and N. G. Kantharia

National Centre for Radio Astrophysics, Tata Institute of Fundamental Research, Post Bag 3, Ganeshkhind, Pune 411007, India

Version 2008 Sep. 25

ABSTRACT

We present deep multifrequency observations using the Giant Metrewave Radio Telescope at 153, 244, 610 and 1260 MHz of a field centered on J0916+6348, to search for evidence of fossil radio lobes which could be due to an earlier cycle of episodic activity of the parent galaxy, as well as halos and relics in clusters of galaxies. We do not find any unambiguous evidence of episodic activity in a list of 374 sources, suggesting that such activity is rare even in relatively deep low-frequency observations. We examine the spectra of all the sources by combining our observations with those from the Westerbork Northern Sky Survey, NRAO VLA Sky Survey and the Faint Images of the Radio Sky at Twenty-centimeters survey. Considering only those which have measurements at a minimum of three different frequencies, we find that almost all sources are consistent with a straight spectrum with a median spectral index, $\alpha \sim 0.8$ ($S(\nu) \propto \nu^{-\alpha}$), which appears steeper than theoretical expectations of the injection spectral index. We identify 14 very steep-spectrum sources with $\alpha \geq 1.3$. We examine their optical fields and discuss the nature of some of these sources.

Key words: Radio continuum: galaxies – galaxies: active – galaxies: clusters: general

1 INTRODUCTION

Low-frequency radio observations of radio galaxies and quasars provide us with an opportunity to probe episodic activity in active galactic nuclei (AGN) and also constrain the injection spectral indices of the electron energy spectrum. The extended radio emission in radio galaxies and quasars could provide constraints on the duration and duty cycles of episodic activity in AGN via the structural and spectral information of the lobes of emission. The most striking examples of such episodic nuclear activity are the ‘double-double’ radio galaxies (DDRGs) where a young pair of radio lobes is seen closer to the nucleus in addition to the older and more distant lobes of emission (e.g. Subrahmanyam, Saripalli & Hunstead 1996; Lara et al. 1999; Schoenmakers et al. 2000; Saikia, Konar & Kulkarni 2006 and references therein). In addition to the DDRGs, diffuse relic radio emission due to an earlier cycle of activity has also been suggested for a number of sources from structural

and spectral information. Some of the examples are 3C338 and 3C388 (Burns, Schwendeman & White 1983; Roettiger et al. 1994), Her A (Gizani & Leahy 2003), 3C310 (van Breugel & Fomalont 1984; Leahy, Pooley & Riley 1986), Cen A (Burns, Feigelson & Schreier 1983; Clarke, Burns & Norman 1992; Junkes et al. 1993; Morganti et al. 1999), and more recently 4C29.30 (Jamrozy et al. 2007). Jeyakumar et al. (2000) have listed a few cases of small-scale halos associated with the known milliarcsec-scale structures of compact steep spectrum and giga-hertz peaked spectrum sources from interplanetary scintillation observations with the Ooty Radio Telescope at 327 MHz. However, examples of such features appear to be relatively rare, and several searches for relic emission around bright radio sources have not yielded positive results (e.g. Reich, Stute & Wielebinski 1980; Stute, Reich & Kalberla 1980; Perley, Fomalont & Johnston 1982; Kronberg & Reich 1983; van der Laan, Zieba & Noordam 1984; Jones & Preston 2001).

The diffuse relic emission is expected to have a steep radio spectrum due to radiative losses and remain visible for approximately $\sim 10^8$ yr (e.g. Owen, Eilek & Kassim 2000;

^{*} Email: sirothia@ncra.tifr.res.in (SKS), djs@ncra.tifr.res.in (DJS), ishwar@ncra.tifr.res.in (CHI) and ngk@ncra.tifr.res.in (NGK)

Table 1. Observation summary and image parameters

	Center Frequency	153 MHz	244 MHz	610 MHz	1260 MHz
General	Date	2005 Dec 12	2005 Nov 26	2005 Nov 26	2008 Apr 22
	Working antennas	29	26	27	27
	Bandwidth	5.6 MHz	32 MHz	32 MHz	32 MHz
	Polarization	RR, LL	LL	RR	RR, LL
	Visibility integration time (s)	16.78	16.78	16.78	4.19
	Total observation time (hr)	7.61	8.57	8.57	6.50
Flux	Source	3C147	3C147	3C147	3C147
Calibrator	Time (hr)	1.01	0.25	0.25	0.26
	Flux density (Jy)	68.29	59.16	38.27	15.58
	Scale	Perley-Taylor 99	Perley-Taylor 99	Perley-Taylor 99	Perley-Taylor 99
Phase	Source	3C147	J0834+5534	J0834+5534	J0834+5534
Calibrator	Time (hr)	1.0	1.72	1.72	0.74
	Flux density (Jy)	68.29	8.60	8.22	7.39
Target	Phase center	J0916+6348	J0916+6348	J0916+6348	J0916+6348
Field	Time (hr)	6.60	6.60	6.60	5.34
	Image size	6144 × 6144	6144 × 6144	6144 × 6144	6144 × 6144
	Pixel size	4'' × 4''	3'' × 3''	2'' × 2''	1'' × 1''
	Rms noise [†] μJy beam ⁻¹	≈ 513	≈ 173	≈ 32	≈ 22
	Synthesized beam	21.48'' × 18.41''	12.09'' × 10.80''	5.51'' × 4.59''	2.85'' × 2.13''
	PA	45.8°	57.4°	47.2°	-47.1°
Primary Beam	Gaussian, FWHM	173.8'	117.0'	42.7'	26.4'
correction parameter	Reference Frequency	153 MHz	235 MHz	610 MHz	1280 MHz

[†] The rms noise given is the median value of all estimates across the primary beam till 20 per cent of the peak response, before primary beam correction.

Kaiser & Cotter 2002; Jamrozy et al. 2004). Low-frequency observations with low rms noise values and short spacings sensitive to the diffuse emission could provide better constraints on the frequency of occurrence or detection of such relic emission. We explore this possibility from observations of a field centered on RA: 09^h 16^m 30^s, DEC: 63° 48' 00'' at a number of frequencies, namely 150, 244, 610 and 1260 MHz, with the Giant Metrewave Radio Telescope (GMRT). This field was chosen when several interesting radio sources, including a wide-angle tailed source, were noticed while studying the nearby group of galaxies Holmberg 124 (Kantharia et al. 2005). In order to identify diffuse cluster sources, it is important that the imaged field contains galaxy clusters. In these observations, the clusters Abell 764 at a redshift of 0.166 (Abell et al. 1989) and MaxBCG J139.14754+63.8034 at a redshift of 0.1215 (Koester et al. 2007) are both very close to the pointing centre.

Deep low-frequency observations are also extremely useful for identifying radio halos, relics and core-halos or mini halos associated with clusters of galaxies. While core-halos are less than about 500 kpc in extent and associated with the dominant galaxy in cooling core clusters, halos and relics are much larger in size and not associated with any particular galaxy. Radio halos are usually projected towards the cluster center and have a regular morphology, while relics are seen towards the periphery with a variety of shapes (cf. Venturi et al. 2008 and references therein). While relics are believed to arise due to cluster mergers and/or matter accretion (Sarazin 1999; Ryu et al. 2003; Pfrommer et al. 2006; Giacintucci et al. 2008), the models for halos range from re-acceleration due to turbulence (Brunetti 2003; Sarazin 2004; Petrosian & Bykov 2008; Brunetti et al. 2007 and references

therein) to production of relativistic electrons by hadronic collisions (e.g. Dolag & Enßlin 2000 and references therein).

In addition to the search for fossil or relic radio emission of different forms, it is also useful to examine the low-frequency spectra of these weak sources, which could be close to their injection spectral indices, α_{inj} (flux density, $S \propto \nu^{-\alpha}$), and compare these with values for stronger sources. Most of our sources are weak and are not catalogued in the well-known low-frequency surveys such as the Cambridge surveys at 151 MHz (Green 2002 and references therein) and the VLA Low-frequency Sky Survey (VLSS; Cohen et al. 2007; <http://lwa.nrl.navy.mil/VLSS>). In the case of the strong sources, α_{inj} has been estimated to be 0.5 for Cygnus A. Similar values have been obtained by Meisenheimer et al. (1989) for a sample of powerful radio galaxies. From measurements between 38 MHz and 1 GHz, Liu, Pooley & Riley (1992) find a median value of 0.77. For a sample of 3CR sources Leahy et al. (1989) estimate the hot spot spectral indices, which are similar to α_{inj} , to have a similar median value of ∼0.8. This is also similar to the estimate of α_{inj} for the compact steep spectrum source 3C190 by Katz-Stone & Rudnick (1997). For a sample of giant radio sources, using low-frequency GMRT observations and higher frequency observations from the Very Large Array (VLA) as well as data from the literature, Jamrozy et al. (2008) find that α_{inj} varies from ∼0.55 to 0.88 with a median value of ∼0.6. The theoretically expected values are somewhat smaller. For a strong, non-relativistic shock in a Newtonian fluid $\alpha_{\text{inj}} = 0.5$ (Bell 1978a, 1978b; Blandford & Ostriker 1978), while the values range from 0.35 to 0.65 for relativistic shocks in

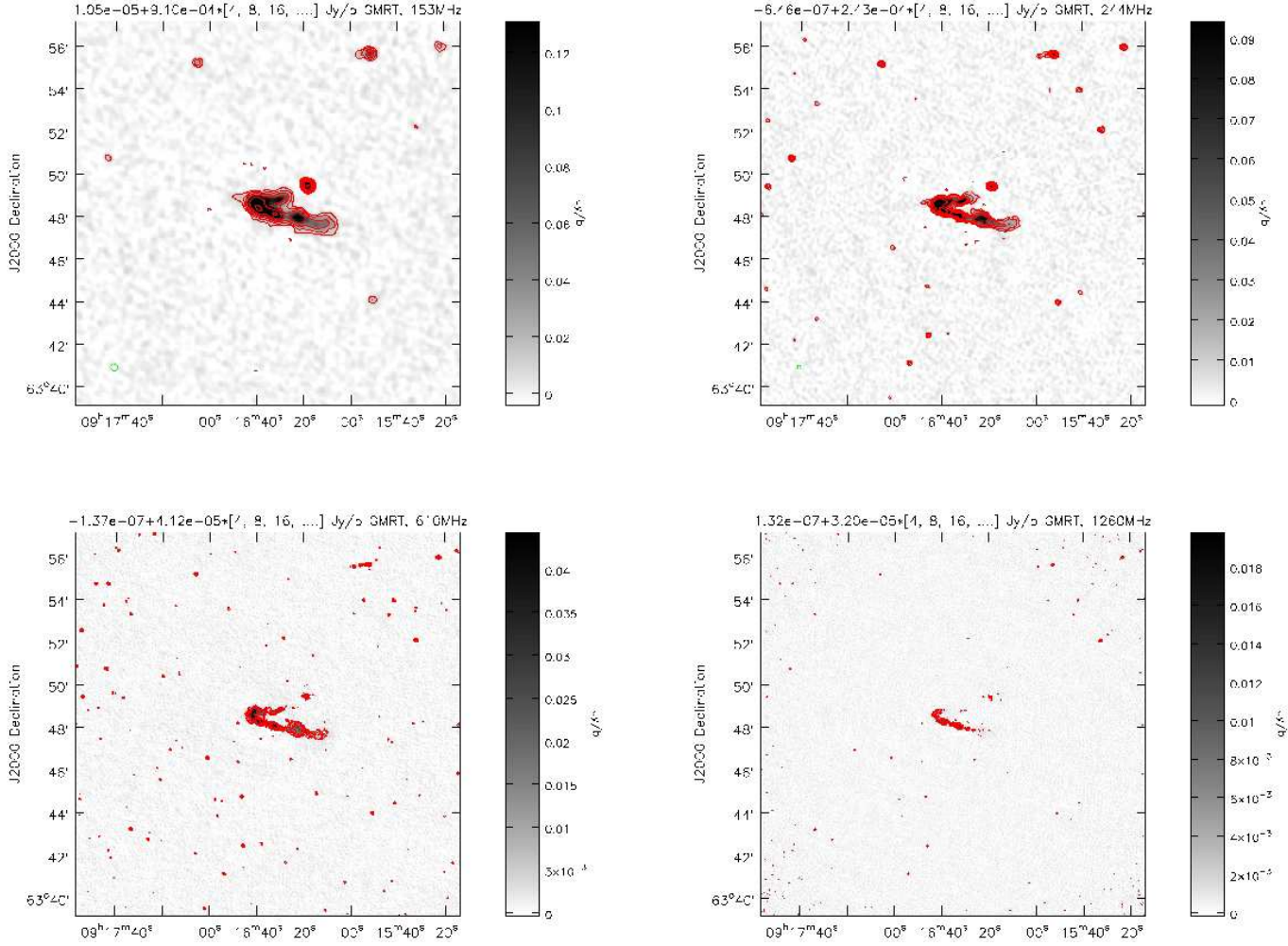


Figure 1. GMRT images of an area of 18×18 arcmin 2 of the field J0916+6348 at 150, 244, 610 and 1260 MHz. The resolutions and rms noise values are listed in Table 1. In this figure and in all the images presented here, the contour levels in units of Jy beam $^{-1}$ are represented by mean+rms \times (n), where n is the multiplication factor. The negative contours are shown as dashed lines.

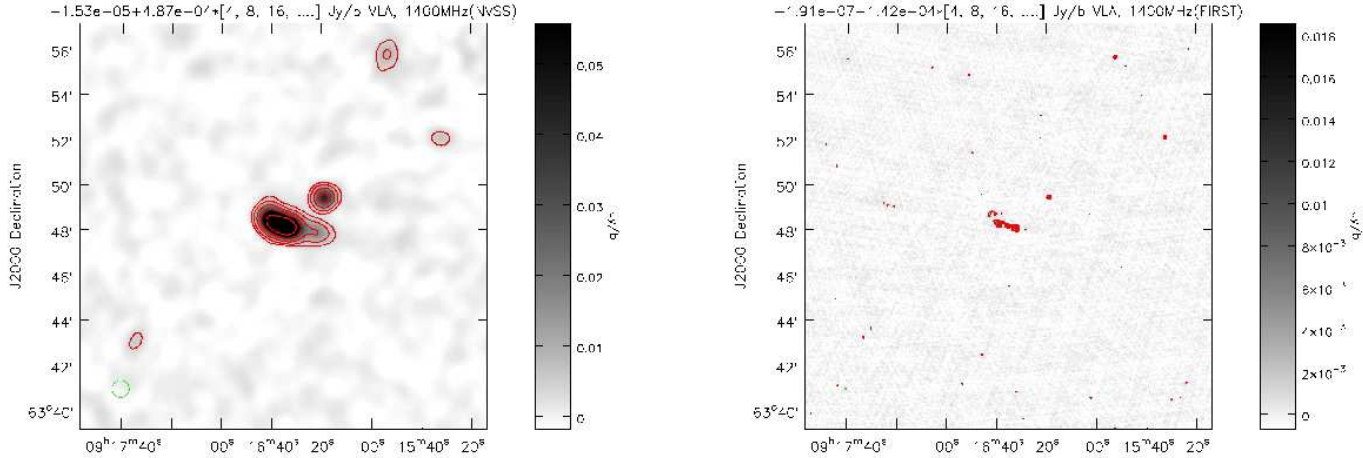


Figure 2. The NVSS (left) and FIRST (right) images of the same area shown in Fig. 1 of the field J0916+6348 at 1400 MHz with angular resolutions of 45 and 5 arcsec respectively. Contour levels: mean+rms \times (n) in units of Jy beam $^{-1}$.

different situations (Heavens 1989; Kirk & Schneider 1987; Drury & Voelk 1981; Axford, Leer & McKenzie 1982).

A summary of the observations and the parameters of the images obtained are presented in Table 1, while the details of our observations and analysis are described in Section 2. The results are presented in Section 3. The discussion and conclusions are summarized in Section 4.

2 OBSERVATIONS AND DATA REDUCTION

The observation summary along with the calibrators used, and the parameters of the final images are presented in Table 1. The data reduction was done mainly using AIPS++ (version: 1.9, build #1556). 3C147 was the primary flux density and bandpass calibrator at all the four frequencies. After applying bandpass corrections on the mentioned phase calibrator, gain and phase variations were estimated, and then flux density, bandpass, gain and phase calibration from flux density and phase calibrator were applied on the target field.

While calibrating the data, bad data were flagged at various stages. The data for antennas with high errors in antenna-based solutions were examined and flagged over certain time ranges. Some baselines were flagged based on closure errors on the bandpass calibrator. Channel and time-based flagging of data points corrupted by radio frequency interference (RFI) were done using a median filter with a 6σ threshold. Residual errors above 5σ were also flagged after a few rounds of imaging and self calibration. The system temperature (T_{sys}) was found to vary with antenna, the ambient temperature and elevation (Sirothia 2008). In the absence of regular T_{sys} measurements for GMRT antennas, this correction was estimated from the residuals of corrected data with respect to the model data. The corrections were then applied to the data. The final image was made after several rounds of phase self calibration, and one round of amplitude self calibration, where the data were normalized by the median gain for all the data. The final image was also primary beam corrected using the Gaussian parameters as mentioned in Table 1.

3 OBSERVATIONAL RESULTS

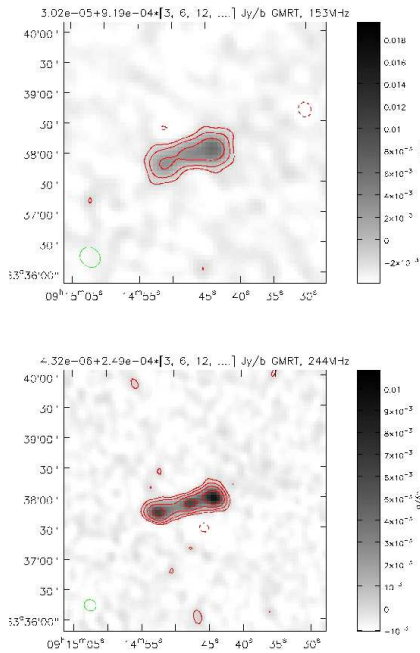
The GMRT images of an area of $\sim 18 \times 18$ arcmin 2 at all the four frequencies are shown in Fig. 1, while the images from the NRAO VLA Sky Survey (NVSS; Condon et al. 1998) and Faint Images of the Radio Sky at Twenty-centimeters survey (FIRST; Becker et al. 1995) are shown in Fig. 2. Amongst the GMRT images, the 1260-MHz image has the lowest noise figure with an rms of about $22 \mu\text{Jy beam}^{-1}$, while the corresponding values for the 150-MHz, 244-MHz and 610-MHz images are 513, 173 and $32 \mu\text{Jy beam}^{-1}$ respectively. Diffuse relic emission with a brightness of $20 \mu\text{Jy beam}^{-1}$ at 1260 MHz and a spectral index, $\alpha \sim 1.5$, would have a surface brightness of ~ 480 and $150 \mu\text{Jy beam}^{-1}$ at 150 and 244 MHz respectively for a similar beam. Considering that our beam areas at these two frequencies are larger than at 1260 MHz by ~ 100 and 50 times respectively, we should be able to detect diffuse relic emission associated with these sources at the lower frequencies even if these were below the threshold at 1260 MHz.

To examine the detection of such diffuse relic emission from either an earlier cycle of activity in a radio galaxy or from cluster relics and halos, and also estimate the low-frequency spectra of these sources, we compiled a list of sources which are within 1.5° of the phase center of our observations at 153 MHz, and with a peak brightness which is at least 6 times larger than the local rms value. This yielded a list of 374 sources. For each of these sources we attempted to find counterparts at the other frequencies of observations as well as in the Westerbork Northern Sky Survey at 327 MHz (WENSS; Rengelink et al. 1997; de Bruyn et al. 2000) when available, and from NVSS and FIRST at 1400 MHz by searching within a radius of 30 arcsec of each source. The search radius was arrived at by comparing the positions of compact sources in the different catalogues.

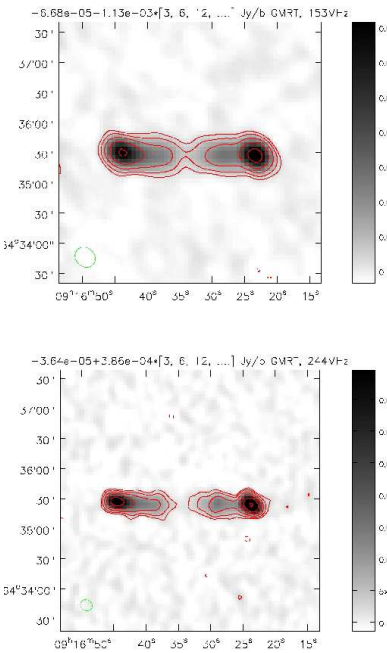
Of these 374 sources, 361 were found to have counterparts at 244 MHz. The remaining 13 sources are located between $\sim 1.06^\circ$ and 1.46° from the pointing center, the median value being $\sim 1.38^\circ$. The primary beam response of the 244-MHz beam at 1.5° from the phase center being about 20 per cent of the peak value, the rms noise is larger. We have checked the field of each of these 13 sources and find that these sources are visible in the 244-MHz image but do not satisfy our selection criterion of the peak value being ≥ 6 times the rms value. Four of these sources are detected in either the NVSS or FIRST catalogues. We have examined the spectra of these sources, but given the uncertainties there is no clear example of a very steep spectrum source amongst these objects.

The sources with a spectral index greater than 1.3 estimated from measurements at a minimum of three frequencies are listed in Table 2 along with some of their observed properties. The Table for the entire list of sources is available in the on-line version. The Tables are arranged as follows. Column 1: source name in J2000 co-ordinates where hhmmss represents the hours, minutes and seconds of right ascension and ddmmss represents the degrees, arcmin and arcsec of declination, estimated from the flux-density weighted centroid of all the emission enclosed by the 3σ contour at 153 MHz; columns 2 and 3: the right ascension and declination of the source in J2000 co-ordinates; column 4: distance of the centroid of the source in the 150-MHz image from the pointing center in degrees; columns 5 to 10: the total flux densities at 153, 244, 330, 610, 1260 and 1400 MHz in units of mJy; column 11: spectral index from a linear least-squares fit for which the spectrum could be satisfactorily fitted with a straight spectrum. For sources which show a strong departure from a straight-line fit, a parabolic form $\log S = b(\log\nu)^2 + m\log\nu + c$ was fitted and the high frequency spectral indices between 610 and 1400 MHz have been quoted. The flux densities at 330 MHz are from the WENSS catalogue while those at 1400 MHz are from the NVSS catalogue. The flux densities from the GMRT observations at 610 and 1260 MHz have been listed for only those sources which are 0.54° and 0.34° of the phase center, which corresponds to about 20 per cent of the peak response of the primary beam. The flux densities of the sources in all the GMRT images have been estimated by integrating the emission within the 3σ closed contour. We have also examined the structure of each source at each frequency as well as in the FIRST and NVSS images. We have not listed the flux densities of a few extended sources at specific frequencies if

GMRT091446+633757



GMRT091633+643528



GMRT092234+640556

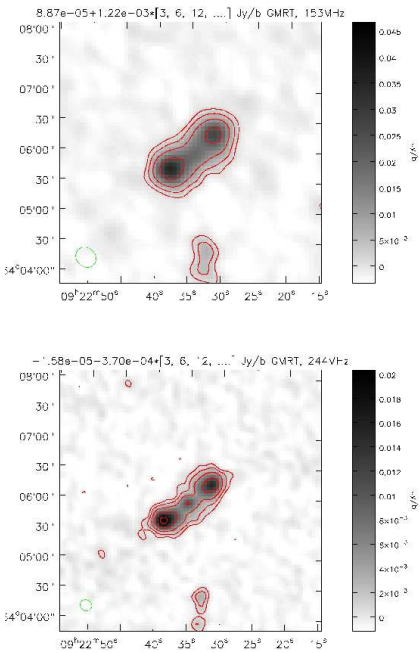


Figure 3. The GMRT images of three double-lobed objects at 153 and 244 MHz. The images of the sources at 153 MHz are in the first row, while the corresponding images of the same source at 244 MHz are in the second row. Contour levels: mean+rms×(n) in units of Jy beam^{-1} .

significant flux density appears to be missing in the images at the given frequency even after convolving it to a lower resolution. This has been done for a few sources at 610 and 1260 MHz. Column 12: structural classification where S denotes a single source, D a double-lobed source, T a triple source with a possible core component and Cplx a complex source. Diffuse extended emission without a clear double-lobed structure has been marked as E. The structural classification has been usually done from the highest resolution image available, which is usually our GMRT image at either 610 or 1260 MHz or the FIRST image at 1400 MHz. The resolution of our 610-MHz image is similar to that of the FIRST image although the noise in our image is significantly better than that of FIRST. We have estimated the errors in the flux densities to be ~ 15 per cent at 150 and 244 MHz, 10 per cent at 610 MHz and 5 per cent at the higher frequencies. For each source we have estimated the error in the value of the spectral index, and find the typical error to be ~ 0.15 .

4 DISCUSSION

4.1 Search for relic emission

Relic radio emission associated with an earlier cycle of activity may be seen as either lobes of emission beyond the extent of the younger lobes as in the case of the double-double radio galaxies, or just diffuse emission associated with a smaller-scale double-lobed or triple radio source. If the relic radio emission, which is likely to have a steep radio spectrum con-

tributes a significant amount of the total flux density one might also find signatures of it in the integrated spectra of these sources. There could also be relic sources without any recent activity; these sources are likely to have a very steep radio spectrum due to radiative losses.

We have examined the structure and spectra of each source in our entire list of 374 sources. Of these, 295 are classified as single, 61 as double, 9 as triple and the remaining 9 as complex sources. Although tails and bridges have been detected in many of the sources, there are no clear unambiguous signatures of episodic activity either in the form of DDRGs or diffuse emission associated with the double-lobed or single sources. The images of three of the large angular-sized, double-lobed sources at both 153 and 244 MHz are shown in Fig. 3. This suggests that sources with clear signatures of episodic activity are rather rare even in fields selected and observed with high sensitivity at a low frequency. We made low-resolution images at the different frequencies to ensure that we have not missed any diffuse steep-spectrum emission.

Most of the known dozen or so DDRGs are associated with large radio galaxies, with sizes typically over about a Mpc (e.g. Schoenmakers et al. 2000; Saikia et al. 2006). This may be due to the typical time scales of episodic activity which have been estimated to be in the range of $\sim 10^7$ – 10^8 yr (Schoenmakers et al. 2000; Konar et al. 2006; Jamrozy et al. 2008; Safouris et al. 2008). About 79 per cent of our sources are single sources, with the median value of angular size for the entire list of sources being less than 10 arcsec, which corresponds to a linear size of only ~ 60 and 80 kpc respectively at redshifts of 0.5 and 1 respectively. The

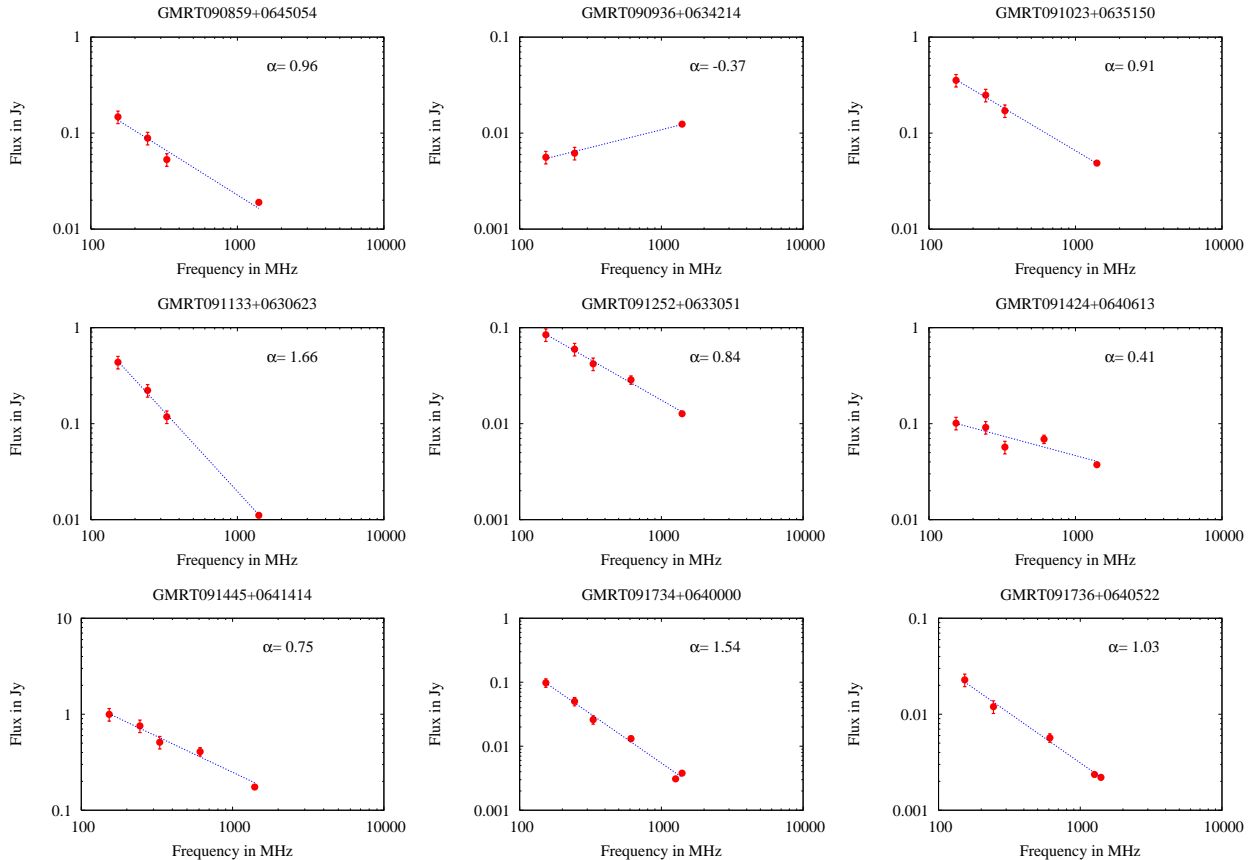


Figure 4. Representative spectra of a few objects fitted with a linear least-squares fit.

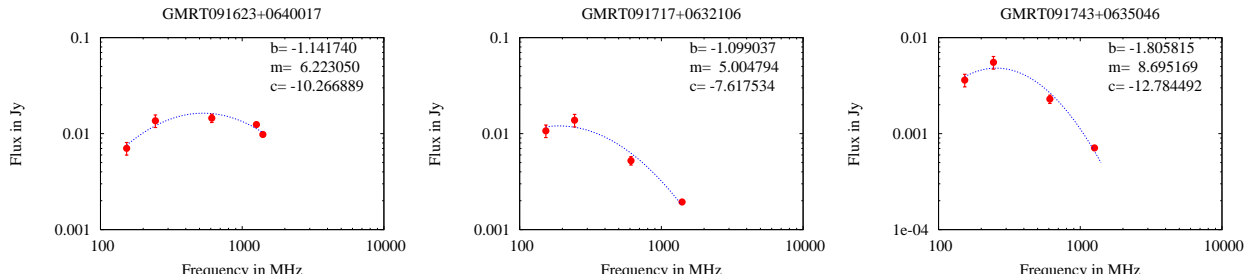


Figure 5. Spectra of the three objects fitted with a parabolic form.

non-detection of unambiguous signatures of episodic activity in these sources may possibly also be related to their small linear sizes and hence younger ages.

4.2 Spectra

We have fitted the spectra for 317 of the sources which have measurements at a minimum of three different frequencies. Since the measurements cover only about a decade in frequency and the number of independent flux density estimates at different frequencies is also limited, we have fitted a straight spectrum to the sources unless the data show evidence of large deviations. The representative spectra of a

few sources with straight spectra are shown in Fig. 4, while those for the three sources with curved spectra are shown in Fig. 5. The curved spectra appear to exhibit turnover frequencies ranging from ~ 100 to 600 MHz. The three sources with a possible low-frequency turnover in their spectra also do not have any extended emission associated with it. The distribution of spectral indices for all the sources is shown in Fig. 6. For the three sources with curved spectra, we have plotted the high-frequency spectral index. The median value of spectral index ~ 0.82 , which is similar to estimates for the powerful 3CR sources (Liu et al. 1992; Leahy et al. 1989; Katz-Stone & Rudnick 1997), but somewhat larger than the theoretically expected values of injection spectral indices discussed earlier.

Table 2. The steep-spectrum sources with a spectral index steeper than 1.3. The Table for the entire list of sources with spectral index information is available in the on-line version.

Source name	RA hh:mm:ss.s	DEC dd:mm:ss.s	Dis deg.	S ₁₅₃ mJy	S ₂₄₄ mJy	S ₃₃₀ mJy	S ₆₁₀ mJy	S ₁₂₆₀ mJy	S ₁₄₀₀ mJy	α	Class
(1)	(2)	(3)	(4)	(5)	(6)	(7)	(8)	(9)	(10)	(11)	(12)
GMRT090357+640848	09:03:57.8	64:08:48.2	1.43	427.0	202.4	139.0	—	—	25.1	1.31	S
GMRT090740+642941	09:07:41.0	64:29:41.4	1.19	53.3	30.4	—	—	—	2.8	1.33	D
GMRT090842+642154	09:08:42.4	64:21:54.2	1.03	102.3	57.2	32.0	—	—	6.0	1.31	S
GMRT091133+630623	09:11:33.4	63:06:23.5	0.89	436.8	222.1	118.0	—	—	11.1	1.66	D
GMRT091308+633945	09:13:08.5	63:39:45.8	0.41	19.1	4.9	—	0.7	—	—	2.37	S
GMRT091328+640209	09:13:28.4	64:02:09.1	0.41	7.6	3.9	—	1.1	—	—	1.37	S
GMRT091734+640001	09:17:34.2	64:00:01.0	0.23	98.2	50.2	26.0	13.1	3.1	3.8	1.54	S
GMRT091744+630229	09:17:44.0	63:02:29.5	0.77	20.6	11.5	—	—	—	1.1	1.34	S
GMRT091845+642854	09:18:45.5	64:28:54.4	0.72	62.4	32.9	17.0	—	—	2.5	1.48	D
GMRT092004+633626	09:20:04.4	63:36:26.5	0.43	22.5	8.6	—	2.9	—	—	1.49	S
GMRT092009+641550	09:20:09.6	64:15:50.1	0.60	256.5	145.9	94.0	—	—	14.4	1.30	S
GMRT092131+633939	09:21:31.9	63:39:39.6	0.57	114.2	60.5	40.0	—	—	4.0	1.50	D
GMRT092332+633611	09:23:32.4	63:36:11.9	0.80	89.0	48.6	38.0	—	—	4.6	1.31	Cplx
GMRT092830+634748	09:28:30.7	63:47:48.8	1.32	96.8	33.1	23.0	—	—	—	1.95	E

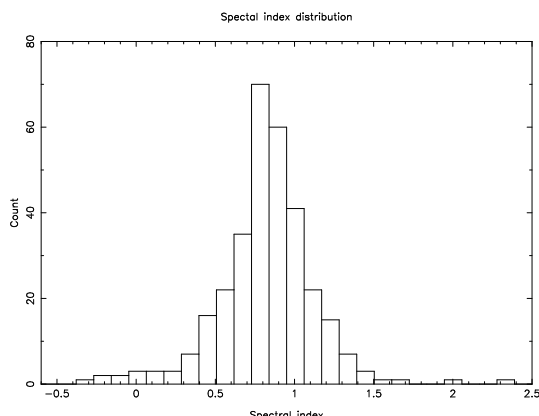


Figure 6. The spectral index distribution for all the 317 sources with a minimum of three measurements at different frequencies. For the three sources fitted with a parabolic form, the high-frequency spectral index between 610 and 1400 MHz has been plotted.

4.3 Very steep spectrum sources

The relic lobes of radio sources from an earlier cycle of activity which are no longer being fed with energy from the nucleus are expected to have a very steep radio spectrum due to radiative losses. For a source with a typical spectral index of 0.8, the expected spectral index beyond the break due to synchrotron ageing is expected to be about 1.3 (Pacholczyk 1970; Parma et al. 2007). The 14 objects from our list with at least three measurements, and spectral indices >1.3 are listed in Table 2. We have confirmed the steep spectra of these sources by convolving the higher resolution images to those of the lower resolution ones. This shows that the number of very steep spectrum sources comprises only ~ 3.7 per cent of our entire list of 374 objects. There have been earlier searches for such steep spectrum sources with the primary objective of finding high-redshift radio galaxies (e.g. Roettgering et al. 1994; De Breuck et al. 2000). These studies also indicate that very steep spectrum sources are rather

rare. For example, in the study by De Breuck et al. (2000), only 0.5 per cent of a complete low-frequency selected sample is found to have a spectral index >1.3 . Our detection rate is somewhat higher because our pointing centre is close to two clusters of galaxies. Radio galaxies in clusters are known to have steeper spectra (e.g. Slee et al. 1983; Roland et al. 1985; Slee & Reynolds 1984), possibly due to confinement of the radio emitting plasma by the intracluster medium. Also, clusters are known to often harbour steep-spectrum relics and halos of emission (cf. Venturi et al. 2008 and references therein).

These sources exhibit structures ranging from single sources to double-lobed and diffuse extended sources. The GMRT images at 153 and 244 MHz of six of these sources are shown in Fig. 7. We have examined the optical fields of each of the 14 sources in the Sloan Digital Sky Survey (Adelman-McCarthy et al. 2008). We have tried to find optical counterparts of these sources as well attempt to identify any cluster of galaxies that might be associated with the radio sources. We have plotted the positions of the galaxies from the SDSS on the radio images, and have described it as a possible identification if the optical object lies within the radio source and is within a few arcsec of the radio centroid.

Of the 14 sources, three (GMRT091308+633945, GMRT092009+641550 and GMRT092131+633939) have possible identifications, and three of the remaining sources (GMRT091734+640001, GMRT091845+0642854, GMRT092830+0634748) are in the directions of clusters of galaxies. These are described briefly here.

GMRT091308+633945: This is a single point source at 610 MHz. The nearest optical galaxy from the SDSS catalogue is J091309.5+633943.0, which is 0.9 arcsec from radio source at 610 MHz. Its r magnitude is 22 and its estimated redshift ranges from 0.1 to 0.77.

GMRT091734+640001: This source has an extension toward the south with an overall size of 19.2 arcsec at 610 MHz. The object is at distance of 10.9 arcmin from the cluster Abell 0764 cluster which is centered at $09^{\text{h}}17^{\text{m}}09.7^{\text{s}}$, $63^{\circ}49'26.4''$. The cluster diameter is about 28 arcmin and is at $z=0.166$ with an x-ray flux density in the 0.1-2.4keV

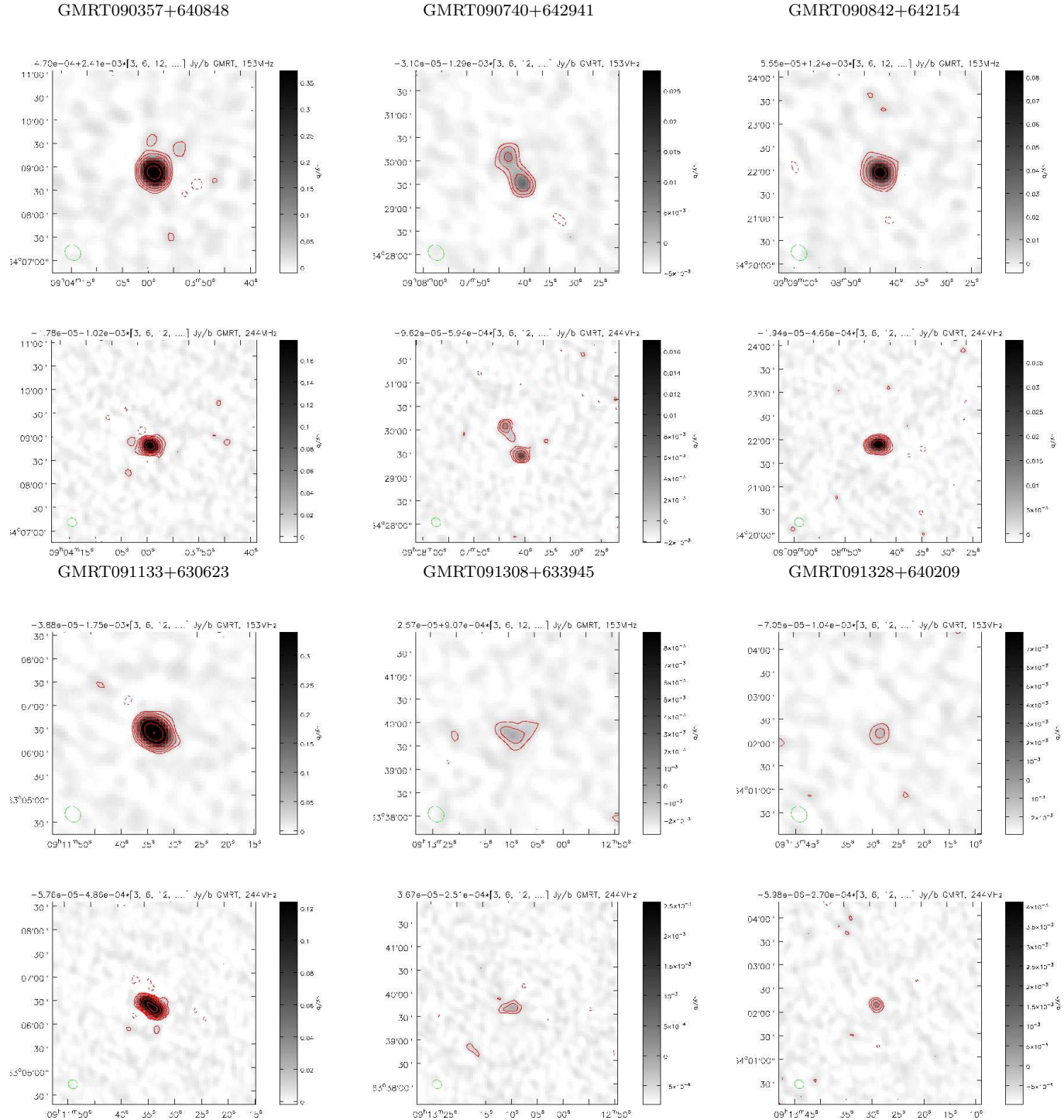


Figure 7. The GMRT images of the very steep spectrum objects at 153 and 244 MHz. The images of the sources at 153 MHz are in the first and third rows, while the corresponding images of the same sources at 244 MHz are in the second and fourth rows. Contour levels: mean+rms \times (n) in units of Jy beam $^{-1}$.

band of $0.904 \times 10^{-15} \text{ W/m}^2$, as listed in the BAX (Base de Données Amas de Galaxies X) X-Ray Galaxy Clusters and Groups Catalog (Sadat et al. 2004).

GMRT091845+0642854: This is a double source with an angular size of 19.9 arcsec at 244 MHz. The object is at a distance of 11.2 arcmin from the Zwicky cluster (Gal et al.

2003) ZW0916+6448 centered at $09^{\text{h}}20^{\text{m}}11.3^{\text{s}}$, $64^{\circ}35'16.8''$. The cluster radius is 0.2° .

GMRT092009+641550: This is a single source with a deconvolved size of 3.92 arcsec from the FIRST catalogue. The nearest optical galaxy from the SDSS catalogue is J092010.8+641548.5, which is located about 2.7 arcsec from

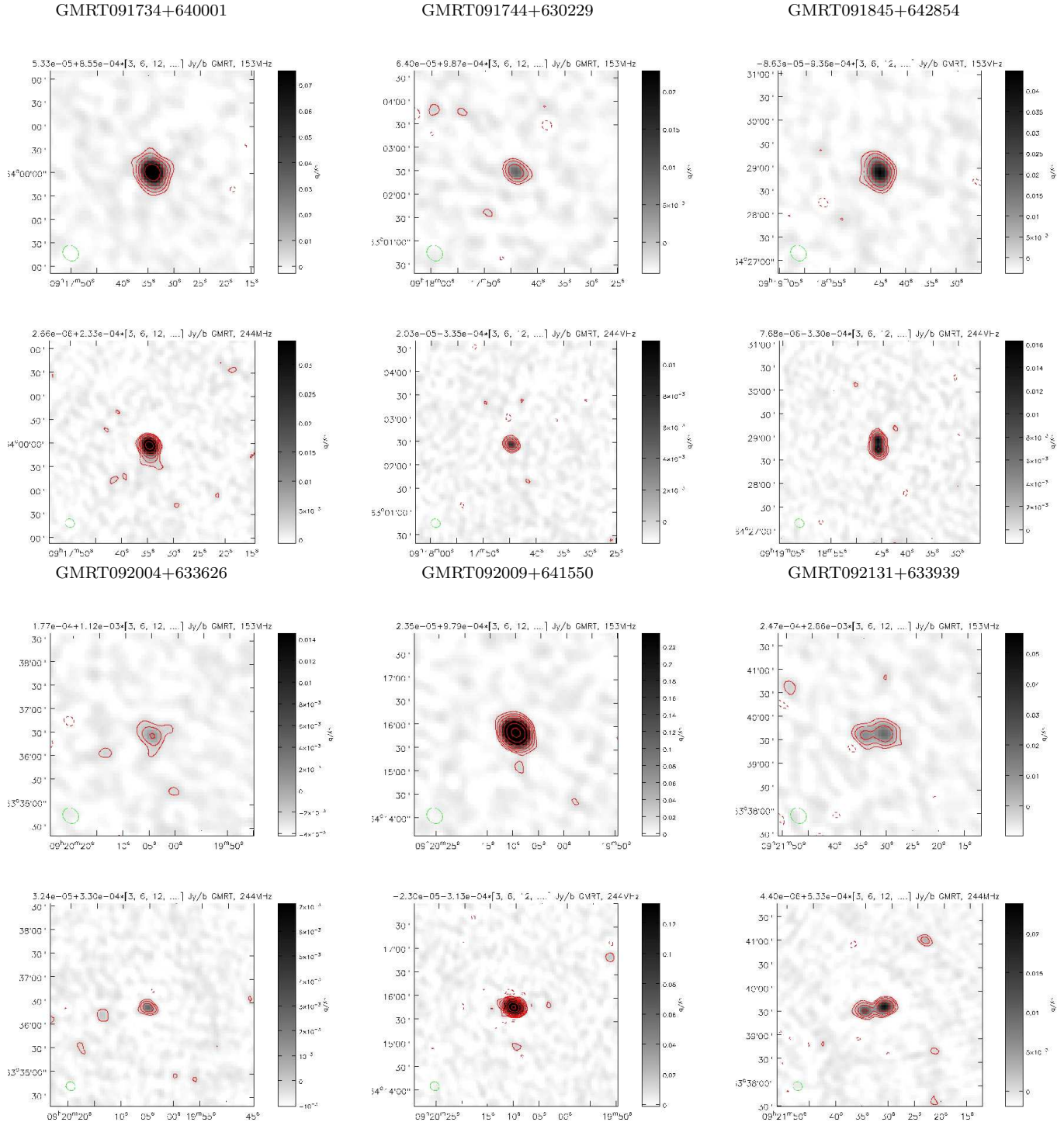
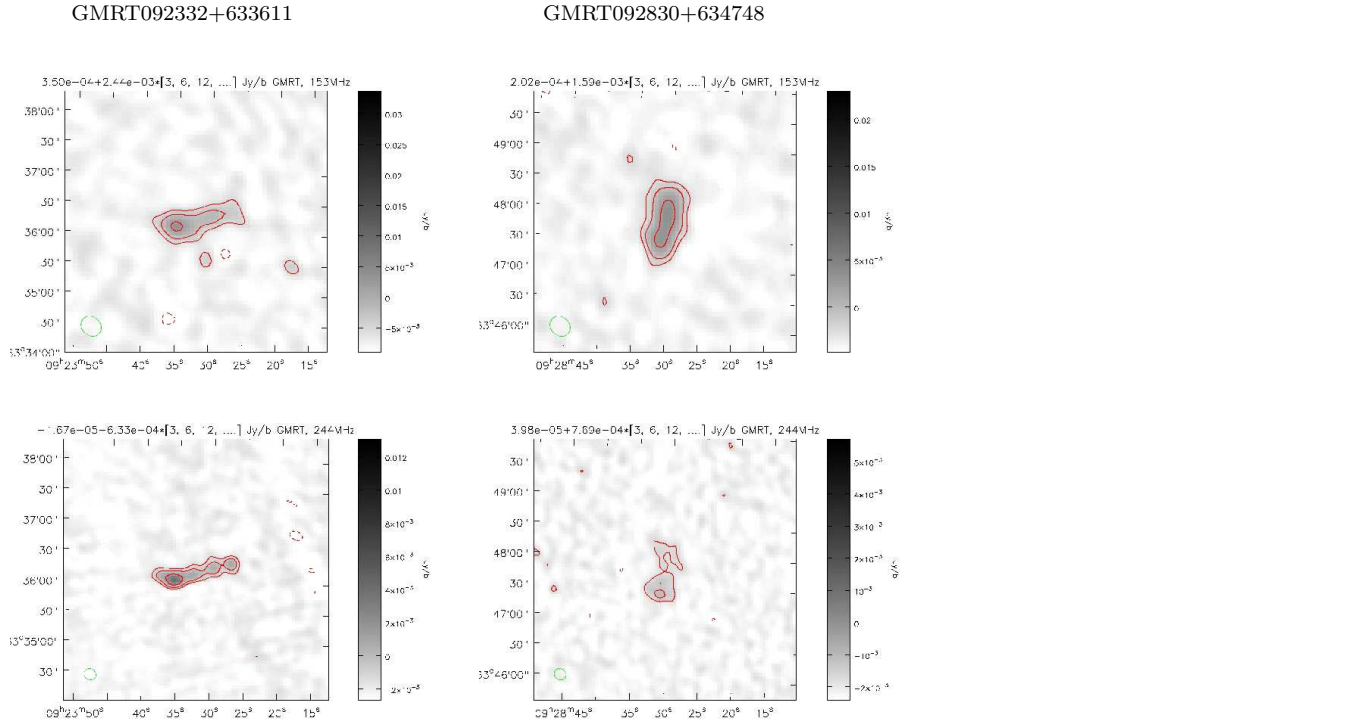


Figure 7 – continued

the FIRST position, has an r magnitude of 22.71 and an estimated photometric redshift of 0.85 ± 0.67 .

GMRT092131+633939: This radio object is an asymmetric double with an angular size of 53.6 arcsec at 244 MHz. The nearest optical galaxy from the SDSS catalogue is J092133.7+633930.7, which is 9.9 arcsec from the centroid and lies between the two radio components. Its r magnitude is 21.52 and its estimated redshift ranges from 0.42 to 0.59.

GMRT092830+0634748: This is a diffuse source with deconvolved size of 13.9 arcsec at 244 MHz. The object is at a distance of 8.2 arcmin from the Zwicky cluster (Gal et al. 2003) ZW0923+6407 centered at $09^{\text{h}}27^{\text{m}}41.0^{\text{s}}$, $63^{\circ}53'56.4''$. The cluster radius is 0.5° .

**Figure 7 – continued**

5 CONCLUDING REMARKS

We have presented deep multifrequency GMRT observations at 153, 244, 610 and 1260 MHz of a field centered on J0916+6348.

We do not find any unambiguous evidence of emission from an earlier cycle of activity in a list of 374 sources, suggesting that such activity is rare even in relatively deep low-frequency observations. However, the median size of our objects is expected to be less than about a 100 kpc, which may be partly responsible for the non-detection of fossil lobes from an earlier cycle of AGN activity.

By combining our flux density measurements with those of WENSS, NVSS and FIRST we find a median spectral index of ~ 0.8 , which is similar to that of the stronger 3CR sources, but appears steeper than theoretical expectations of the injection spectral index.

We identify 14 very steep-spectrum sources with a steep spectral index ≥ 1.3 . We find three of these sources to be identified with an optical galaxy visible in the SDSS, while another three are in the directions of clusters of galaxies. One of these three, GMRT092830+0634748, is a diffuse extended source and could be a cluster relic.

ACKNOWLEDGMENTS

We thank the anonymous referee for his/her helpful comments and the staff of the GMRT who have made these observations possible. GMRT is run by the National Centre for Radio Astrophysics of the Tata Institute of Fundamental Research. This research has made use of the NASA/IPAC Extragalactic Database (NED) which is operated by the Jet

Propulsion Laboratory, California Institute of Technology, under contract with the National Aeronautics and Space Administration.

REFERENCES

- Abell G. O., Corwin Jr. H. G., Olowin R. P., 1989, ApJS, 70, 1
- Adelman-McCarthy J. K., et al., 2008, ApJS, 175, 297
- Axford W. I., Leer E., McKenzie J. F., 1982, A&A, 111, 317
- Becker R. H., White R. L., Helfand D. J., 1995, ApJ, 450, 559
- Bell A. R., 1978a, MNRAS, 182, 147
- Bell A. R., 1978b, MNRAS, 182, 443
- Blandford R. D., Ostriker J. P., 1978, ApJ, 221, L29
- Brunetti G., 2003, in Bowyer S., Hwang C.-Y., eds, Astronomical Society of the Pacific Conference Series Vol. 301 of Astronomical Society of the Pacific Conference Series, Modelling the Non-Thermal Emission from Galaxy Clusters. p. 349
- Brunetti G., Venturi T., Dallacasa D., Cassano R., Dolag K., Giacintucci S., Setti G., 2007, ApJ, 670, L5
- Burns J. O., Feigelson E. D., Schreier E. J., 1983, ApJ, 273, 128
- Burns J. O., Schwendeman E., White R. A., 1983, ApJ, 271, 575
- Clarke D. A., Burns J. O., Norman M. L., 1992, ApJ, 395, 444
- Cohen A. S., Lane W. M., Cotton W. D., Kassim N. E., Lazio T. J. W., Perley R. A., Condon J. J., Erickson W. C., 2007, AJ, 134, 1245

- Condon J. J., Cotton W. D., Greisen E. W., Yin Q. F., Perley R. A., Taylor G. B., Broderick J. J., 1998, AJ, 115, 1693
- De Breuck C., van Breugel W., Röttgering H. J. A., Miley G., 2000, A&AS, 143, 303
- de Bruyn G., et al., 2000, VizieR Online Data Catalog, 8062, 0
- Dolag K., Enßlin T. A., 2000, A&A, 362, 151
- Drury L. O., Voelk J. H., 1981, ApJ, 248, 344
- Gal R. R., de Carvalho R. R., Lopes P. A. A., Djorgovski S. G., Brunner R. J., Mahabal A., Odewahn S. C., 2003, AJ, 125, 2064
- Giacintucci S., Venturi T., Macario G., Dallacasa D., Brunetti G., Markevitch M., Cassano R., Bardelli S., Athreya R., 2008, A&A, 486, 347
- Gizani N. A. B., Leahy J. P., 2003, MNRAS, 342, 399
- Green D. A., 2002, in Pramesh Rao A., Swarup G., Gopal-Krishna eds, The Universe at Low Radio Frequencies Vol. 199 of IAU Symposium, Cambridge Low Frequency Surveys. p. 21
- Heavens A., 1989, in Meisenheimer K., Roeser H.-J., eds, Hot Spots in Extragalactic Radio Sources Vol. 327 of Lecture Notes in Physics, Berlin Springer Verlag, Spectral indices from relativistic and non-relativistic shocks. pp 247–251
- Jamrozy M., Klein U., Mack K.-H., Gregorini L., Parma P., 2004, A&A, 427, 79
- Jamrozy M., Konar C., Machalski J., Saikia D. J., 2008, MNRAS, 385, 1286
- Jamrozy M., Konar C., Saikia D. J., Stawarz Ł., Mack K.-H., Siemiginowska A., 2007, MNRAS, 378, 581
- Jeyakumar S., Saikia D. J., Pramesh Rao A., Balasubramanian V., 2000, A&A, 362, 27
- Jones D. L., Preston R. A., 2001, AJ, 122, 2940
- Junkes N., Haynes R. F., Harnett J. I., Jauncey D. L., 1993, A&A, 274, 1009
- Kaiser C. R., Cotter G., 2002, MNRAS, 336, 649
- Kantharia N. G., Ananthakrishnan S., Nityananda R., Hota A., 2005, A&A, 435, 483
- Katz-Stone D. M., Rudnick L., 1997, ApJ, 479, 258
- Kirk J. G., Schneider P., 1987, ApJ, 315, 425
- Koester B. P., et al., 2007, ApJ, 660, 239
- Konar C., Saikia D. J., Jamrozy M., Machalski J., 2006, MNRAS, 372, 693
- Kronberg P. P., Reich W., 1983, A&A, 125, 146
- Lara L., Márquez I., Cotton W. D., Feretti L., Giovannini G., Marcaide J. M., Venturi T., 1999, A&A, 348, 699
- Leahy J. P., Muxlow T. W. B., Stephens P. W., 1989, MNRAS, 239, 401
- Leahy J. P., Pooley G. G., Riley J. M., 1986, MNRAS, 222, 753
- Liu R., Pooley G., Riley J. M., 1992, MNRAS, 257, 545
- Meisenheimer K., Roser H.-J., Hiltner P. R., Yates M. G., Longair M. S., Chini R., Perley R. A., 1989, A&A, 219, 63
- Morganti R., Killeen N. E. B., Ekers R. D., Oosterloo T. A., 1999, MNRAS, 307, 750
- Owen F. N., Eilek J. A., Kassim N. E., 2000, ApJ, 543, 611
- Pacholczyk A. G., 1970, Radio astrophysics. Nonthermal processes in galactic and extragalactic sources. Series of Books in Astronomy and Astrophysics, San Francisco: Freeman, 1970
- Parma P., Murgia M., de Ruiter H. R., Fanti R., Mack K.-H., Govoni F., 2007, A&A, 470, 875
- Perley R. A., Fomalont E. B., Johnston K. J., 1982, ApJ, 255, L93
- Petrosian V., Bykov A. M., 2008, Space Science Reviews, 134, 207
- Pfrommer C., Springel V., Enßlin T. A., Jubelgas M., 2006, MNRAS, 367, 113
- Reich W., Stute U., Wielebinski R., 1980, A&A, 89, 204
- Rengelink R. B., Tang Y., de Bruyn A. G., Miley G. K., Bremer M. N., Roettgering H. J. A., Bremer M. A. R., 1997, A&AS, 124, 259
- Roettgering H. J. A., Lacy M., Miley G. K., Chambers K. C., Saunders R., 1994, A&AS, 108, 79
- Roettiger K., Burns J. O., Clarke D. A., Christiansen W. A., 1994, ApJ, 421, L23
- Roland J., Hanisch R. J., Veron P., Fomalont E., 1985, A&A, 148, 323
- Ryu D., Kang H., Hallman E., Jones T. W., 2003, ApJ, 593, 599
- Sadat R., Blanchard A., Kneib J.-P., Mathez G., Madore B., Mazzarella J. M., 2004, A&A, 424, 1097
- Safouris V., Subrahmanyam R., Bicknell G. V., Saripalli L., 2008, MNRAS, 385, 2117
- Saikia D. J., Konar C., Kulkarni V. K., 2006, MNRAS, 366, 1391
- Sarazin C. L., 1999, ApJ, 520, 529
- Sarazin C. L., 2004, Journal of Korean Astronomical Society, 37, 433
- Schoenmakers A. P., de Bruyn A. G., Röttgering H. J. A., van der Laan H., Kaiser C. R., 2000, MNRAS, 315, 371
- Sirothia S. K., 2008, MNRAS, submitted
- Slee O. B., Reynolds J. E., 1984, Proceedings of the Astronomical Society of Australia, 5, 516
- Slee O. B., Siegman C. B., Wilson I. R. G., 1983, Australian Journal of Physics, 36, 101
- Stute U., Reich W., Kalberla P. M. W., 1980, A&AS, 42, 299
- Subrahmanyam R., Saripalli L., Hunstead R. W., 1996, MNRAS, 279, 257
- van Breugel W., Fomalont E. B., 1984, ApJ, 282, L55
- van der Laan H., Zieba S., Noordam J. E., 1984, in Fanti R., Kellermann K. I., Setti G., eds, VLBI and Compact Radio Sources Vol. 110 of IAU Symposium, Faint Extended Radio Sources Surrounding Active Galaxy Nuclei. p. 9
- Venturi T., Giacintucci S., Dallacasa D., Cassano R., Brunetti G., Bardelli S., Setti G., 2008, A&A, 484, 327

Table 2. The Table for the entire list of sources with spectral index information (available in online version only).

Source name	RA hh:mm:ss.s	DEC dd:mm:ss.s	Dis deg.	S ₁₅₃ mJy	S ₂₄₄ mJy	S ₃₃₀ mJy	S ₆₁₀ mJy	S ₁₂₆₀ mJy	S ₁₄₀₀ mJy	α	Class
(1)	(2)	(3)	(4)	(5)	(6)	(7)	(8)	(9)	(10)	(11)	(12)
GMRT090312+0640001	09:03:12.9	64:00:01.1	1.48	59.6	32.4	13.0	—	—	11.8	0.77	S
GMRT090336+0633813	09:03:37.0	63:38:13.6	1.45	418.2	235.7	176.0	—	—	49.1	0.99	S
GMRT090353+0633416	09:03:53.7	63:34:16.6	1.43	16.2	6.1	—	—	—	3.0	0.71	S
GMRT090357+0640848	09:03:57.8	64:08:48.2	1.43	427.0	202.4	139.0	—	—	25.1	1.31	S
GMRT090402+0632412	09:04:02.9	63:24:12.9	1.45	36.3	19.3	18.0	—	—	9.6	0.58	S
GMRT090403+0641148	09:04:03.1	64:11:48.3	1.43	17.6	9.2	—	—	—	3.1	0.76	S
GMRT090413+0634054	09:04:13.3	63:40:54.4	1.37	58.3	32.0	29.0	—	—	7.6	0.91	S
GMRT090421+0641502	09:04:21.9	64:15:02.2	1.41	23.8	18.3	—	—	—	6.9	0.56	S
GMRT090425+0640650	09:04:25.8	64:06:50.8	1.37	48.6	28.6	16.0	—	—	8.5	0.81	S
GMRT090444+0634149	09:04:44.7	63:41:49.4	1.31	13.6	7.2	—	—	—	1.4	1.02	S
GMRT090455+0632924	09:04:55.7	63:29:24.0	1.33	108.3	59.8	44.0	—	—	10.7	1.05	S
GMRT090459+0642958	09:04:59.7	64:29:58.6	1.44	7.0	7.8	—	—	—	6.9	0.02	S
GMRT090510+0640149	09:05:10.6	64:01:49.6	1.27	209.1	127.2	73.0	—	—	25.8	0.98	S
GMRT090518+0634333	09:05:18.1	63:43:33.6	1.25	68.6	47.6	34.0	—	—	12.5	0.78	S
GMRT090524+0632512	09:05:24.1	63:25:12.4	1.30	19.0	11.4	—	—	—	25.8	-0.21	S
GMRT090531+0635941	09:05:31.3	63:59:41.9	1.23	38.7	26.5	—	—	—	11.3	0.55	S
GMRT090534+0635639	09:05:34.3	63:56:39.6	1.22	165.3	109.3	79.0	—	—	30.4	0.78	S
GMRT090539+0642121	09:05:39.3	64:21:21.0	1.32	33.9	22.4	15.0	—	—	7.3	0.70	S
GMRT090550+0631447	09:05:50.2	63:14:47.2	1.32	18.4	14.2	—	—	—	3.3	0.78	S
GMRT090604+0642026	09:06:04.4	64:20:26.5	1.27	21.2	15.8	—	—	—	4.1	0.75	S
GMRT090607+0634848	09:06:07.3	63:48:48.5	1.15	692.6	414.1	263.0	—	—	91.3	0.97	D
GMRT090614+0630148	09:06:14.7	63:01:48.6	1.39	38.6	17.5	—	—	—	3.6	1.06	S
GMRT090621+0644304	09:06:21.6	64:43:04.2	1.44	19.7	16.6	—	—	—	3.8	0.76	S
GMRT090624+0631218	09:06:24.1	63:12:18.5	1.28	423.7	355.9	284.0	—	—	82.5	0.72	S
GMRT090641+0643742	09:06:41.4	64:37:42.8	1.36	52.9	23.7	17.0	—	—	7.8	0.87	S
GMRT090645+0635220	09:06:46.0	63:52:20.7	1.08	60.2	39.8	15.0	—	—	8.8	0.92	S
GMRT090645+0640829	09:06:45.5	64:08:29.2	1.13	6.9	4.2	—	—	—	2.0	0.54	S
GMRT090655+0642508	09:06:55.8	64:25:08.2	1.22	32.3	14.8	—	—	—	2.6	1.13	S
GMRT090657+0633704	09:06:57.1	63:37:04.8	1.08	21.8	15.3	—	—	—	4.5	0.71	S
GMRT090704+0641405	09:07:04.5	64:14:05.7	1.13	10.0	6.4	—	—	—	4.8	0.30	S
GMRT090707+0632649	09:07:07.6	63:26:49.6	1.11	81.4	49.8	24.0	—	—	10.0	0.99	S
GMRT090714+0630308	09:07:14.3	63:03:08.6	1.29	36.6	25.8	—	—	—	5.6	0.85	S
GMRT090729+0640339	09:07:29.7	64:03:39.9	1.03	12.6	6.0	—	—	—	2.9	0.63	T
GMRT090731+0643627	09:07:31.2	64:36:27.0	1.27	66.7	47.3	34.0	—	—	9.1	0.90	S
GMRT090733+0642226	09:07:33.2	64:22:26.0	1.14	138.2	84.6	53.0	—	—	20.6	0.88	D
GMRT090740+0642941	09:07:41.0	64:29:41.4	1.19	53.3	30.4	—	—	—	2.8	1.33	D
GMRT090742+0641012	09:07:42.1	64:10:12.3	1.04	33.5	25.5	—	—	—	19.4	0.23	S
GMRT090745+0631759	09:07:45.4	63:17:59.1	1.10	28.4	23.8	16.0	—	—	5.5	0.76	S
GMRT090750+0642030	09:07:50.2	64:20:30.0	1.10	41.6	35.4	27.0	—	—	12.4	0.56	S
GMRT090756+0641856	09:07:56.3	64:18:56.2	1.08	14.6	6.6	—	—	—	2.6	0.75	S
GMRT090808+0624820	09:08:08.5	62:48:20.9	1.38	273.2	144.9	87.0	—	—	25.3	1.12	D
GMRT090816+0625249	09:08:16.1	62:52:49.5	1.31	17.9	10.1	—	—	—	3.1	0.78	S
GMRT090834+0633533	09:08:34.5	63:35:33.1	0.91	20.7	17.6	—	—	—	4.6	0.69	S
GMRT090838+0632257	09:08:38.7	63:22:57.2	0.98	28.7	19.2	—	—	—	3.3	0.98	S
GMRT090839+0635954	09:08:39.6	63:59:54.5	0.89	173.3	134.2	85.0	—	—	30.3	0.81	S
GMRT090842+0641138	09:08:42.4	64:11:38.2	0.95	27.1	14.0	—	—	—	2.1	1.15	S
GMRT090842+0642154	09:08:42.4	64:21:54.2	1.03	102.3	57.2	32.0	—	—	6.0	1.31	S
GMRT090846+0624817	09:08:46.5	62:48:17.9	1.33	319.8	159.8	120.0	—	—	28.5	1.11	D
GMRT090847+0635629	09:08:47.3	63:56:29.5	0.87	73.1	51.8	31.0	—	—	14.3	0.76	S
GMRT090848+0630901	09:08:48.5	63:09:02.0	1.09	549.0	350.2	250.0	—	—	58.9	1.01	S

Table 2 – continued

Source name (1)	RA hh:mm:ss.s (2)	DEC dd:mm:ss.s (3)	Dis deg. (4)	S ₁₅₃ mJy (5)	S ₂₄₄ mJy (6)	S ₃₃₀ mJy (7)	S ₆₁₀ mJy (8)	S ₁₂₆₀ mJy (9)	S ₁₄₀₀ mJy (10)	α (11)	Class (12)
GMRT090859+0640830	09:08:59.4	64:08:30.8	0.90	17.2	11.4	—	—	—	3.7	0.69	S
GMRT090859+0645054	09:08:59.9	64:50:54.6	1.33	147.7	88.6	53.0	—	—	19.0	0.96	S
GMRT090904+0640923	09:09:04.2	64:09:23.6	0.90	22.2	15.4	—	—	—	3.3	0.86	S
GMRT090906+0635117	09:09:06.7	63:51:17.4	0.83	24.3	18.1	—	—	—	6.1	0.62	D
GMRT090909+0623744	09:09:09.4	62:37:44.6	1.44	37.3	18.0	—	—	—	5.2	0.87	S
GMRT090911+0643524	09:09:11.6	64:35:24.2	1.13	455.3	288.5	197.0	—	—	64.9	0.91	S
GMRT090913+0642731	09:09:13.3	64:27:31.2	1.04	29.2	18.3	—	—	—	3.9	0.91	S
GMRT090918+0635958	09:09:18.0	63:59:58.1	0.83	1092.2	710.9	465.0	—	—	159.6	0.91	Cplx
GMRT090922+0631604	09:09:22.3	63:16:04.3	0.97	46.4	33.9	25.0	—	—	7.7	0.82	D
GMRT090923+0650100	09:09:23.8	65:01:00.3	1.44	302.9	167.1	133.0	—	—	37.1	0.96	S
GMRT090926+0634214	09:09:27.0	63:42:14.1	0.80	72.3	50.8	18.0	—	—	7.2	1.11	D
GMRT090936+0634214	09:09:36.4	63:42:14.0	0.78	5.6	6.2	—	—	—	12.4	-0.37	S
GMRT090952+0644549	09:09:52.4	64:45:49.9	1.21	81.0	60.5	32.0	—	—	13.8	0.83	D
GMRT090952+0650625	09:09:52.2	65:06:25.0	1.49	19.8	12.0	—	—	—	3.7	0.75	S
GMRT091002+0625229	09:10:02.4	62:52:29.3	1.18	124.7	66.0	60.0	—	—	10.5	1.09	D
GMRT091007+0633546	09:10:08.0	63:35:46.5	0.74	16.5	12.4	—	—	—	1.1	1.25	S
GMRT091011+0632832	09:10:12.0	63:28:32.4	0.78	14.4	9.0	—	—	—	2.1	0.86	S
GMRT091012+0625309	09:10:12.6	62:53:09.0	1.16	96.4	55.1	—	—	—	11.8	0.95	D
GMRT091012+0645718	09:10:12.9	64:57:18.9	1.34	49.2	29.9	17.0	—	—	8.4	0.82	S
GMRT091016+0634249	09:10:16.0	63:42:50.0	0.70	35.5	24.6	—	—	—	5.8	0.82	D
GMRT091018+0633718	09:10:18.4	63:37:18.5	0.72	27.9	15.7	—	—	—	7.8	0.55	S
GMRT091019+0625558	09:10:19.4	62:55:58.2	1.12	14.1	8.1	—	—	—	2.4	0.79	S
GMRT091021+0623435	09:10:21.1	62:34:35.2	1.41	255.3	121.0	84.0	—	—	17.2	1.24	S
GMRT091023+0635150	09:10:23.4	63:51:50.8	0.69	354.9	248.7	171.0	—	—	48.7	0.91	S
GMRT091051+0625408	09:10:51.6	62:54:08.9	1.11	10.6	7.6	—	—	—	1.5	0.88	S
GMRT091053+0641930	09:10:53.9	64:19:30.8	0.81	676.5	447.7	—	—	—	72.5	1.00	D
GMRT091056+0644151	09:10:56.9	64:41:51.0	1.08	1907.8	1285.5	864.0	—	—	253.5	0.94	S
GMRT091059+0640107	09:10:59.7	64:01:07.7	0.65	248.3	184.3	119.0	—	—	45.1	0.79	S
GMRT091103+0630312	09:11:03.5	63:03:12.2	0.97	26.3	21.9	—	—	—	9.8	0.45	S
GMRT091105+0642013	09:11:05.6	64:20:13.6	0.80	426.6	297.5	—	—	—	52.9	0.94	S
GMRT091117+0630930	09:11:17.9	63:09:30.2	0.87	14.1	16.1	—	—	—	13.0	0.06	S
GMRT091120+0632133	09:11:20.5	63:21:33.6	0.73	34.9	29.3	—	—	—	6.4	0.78	S
GMRT091122+0640813	09:11:22.3	64:08:14.0	0.66	33.3	22.5	—	—	—	4.4	0.92	S
GMRT091126+0642320	09:11:26.2	64:23:20.7	0.81	20.6	14.5	—	—	—	1.5	1.19	S
GMRT091133+0630623	09:11:33.4	63:06:23.5	0.89	436.8	222.1	118.0	—	—	11.1	1.66	D
GMRT091135+0641609	09:11:35.3	64:16:09.8	0.72	16.3	16.5	—	—	—	4.9	0.57	S
GMRT091136+0651054	09:11:36.6	65:10:54.7	1.48	387.9	185.0	139.0	—	—	41.2	1.05	D
GMRT091139+0623918	09:11:39.9	62:39:18.7	1.27	34.5	24.5	—	—	—	9.8	0.56	S
GMRT091153+0633955	09:11:53.7	63:39:55.7	0.54	6.6	5.3	—	3.7	—	2.8	0.39	S
GMRT091154+0644346	09:11:54.0	64:43:46.4	1.06	67.2	50.2	37.0	—	—	12.5	0.77	S
GMRT091157+0632128	09:11:57.6	63:21:28.3	0.68	665.9	489.7	354.0	—	—	122.9	0.77	S
GMRT091201+0632720	09:12:01.1	63:27:20.7	0.61	167.9	107.5	57.0	—	—	15.3	1.12	S
GMRT091205+0630913	09:12:05.7	63:09:13.2	0.82	76.2	47.5	30.0	—	—	7.9	1.04	S
GMRT091212+0634541	09:12:12.5	63:45:41.9	0.49	147.4	106.8	65.0	56.2	—	23.1	0.80	S
GMRT091223+0635840	09:12:23.6	63:58:40.2	0.49	24.2	17.4	—	10.9	—	5.9	0.62	S
GMRT091238+0633330	09:12:38.3	63:33:30.5	0.50	10.0	8.6	—	4.8	—	3.6	0.49	D
GMRT091238+0650419	09:12:38.7	65:04:19.6	1.34	18.8	10.3	—	—	—	4.8	0.59	S
GMRT091246+0634932	09:12:46.1	63:49:32.1	0.42	488.0	298.5	169.0	111.9	—	36.9	1.15	D
GMRT091250+0623803	09:12:50.4	62:38:04.0	1.24	83.3	55.8	42.0	—	—	17.6	0.71	S
GMRT091252+0633051	09:12:52.5	63:30:51.4	0.50	84.5	59.7	42.0	28.6	—	12.7	0.84	S

Table 2 – continued

Source name (1)	RA hh:mm:ss.s (2)	DEC dd:mm:ss.s (3)	Dis deg. (4)	S ₁₅₃ mJy (5)	S ₂₄₄ mJy (6)	S ₃₃₀ mJy (7)	S ₆₁₀ mJy (8)	S ₁₂₆₀ mJy (9)	S ₁₄₀₀ mJy (10)	α (11)	Class (12)
GMRT091256+0625901	09:12:56.7	62:59:01.1	0.92	22.1	17.2	—	—	—	4.8	0.70	S
GMRT091257+0624148	09:12:57.4	62:41:48.9	1.18	59.1	33.4	21.0	—	—	10.8	0.78	S
GMRT091259+0631651	09:12:59.3	63:16:51.2	0.66	7.7	4.3	—	—	—	0.7	1.07	S
GMRT091303+0631808	09:13:03.8	63:18:08.9	0.64	12.2	8.6	—	—	—	2.9	0.65	S
GMRT091306+0630428	09:13:06.7	63:04:28.9	0.83	6.8	5.0	—	—	—	1.3	0.75	S
GMRT091308+0633945	09:13:08.5	63:39:45.8	0.41	19.1	4.9	—	0.7	—	—	2.37	S
GMRT091311+0645419	09:13:11.9	64:54:19.4	1.16	715.6	351.2	234.0	—	—	59.7	1.18	Cplx
GMRT091313+0635126	09:13:14.0	63:51:26.4	0.37	23.1	16.4	—	8.0	—	4.1	0.78	D
GMRT091325+0633032	09:13:25.6	63:30:32.4	0.46	54.3	42.0	23.0	20.1	—	9.2	0.80	S
GMRT091326+0642810	09:13:26.6	64:28:10.9	0.75	59.1	43.1	27.0	—	—	8.9	0.87	S
GMRT091328+0640209	09:13:28.4	64:02:09.1	0.41	7.6	3.9	—	1.1	—	—	1.37	S
GMRT091335+0625203	09:13:35.2	62:52:03.1	0.99	14.9	7.7	—	—	—	3.4	0.64	S
GMRT091336+0631857	09:13:36.0	63:18:57.8	0.59	70.2	45.5	22.0	—	—	13.4	0.78	Cplx
GMRT091337+0630408	09:13:37.5	63:04:08.7	0.81	109.4	66.3	37.0	—	—	11.1	1.07	S
GMRT091342+0630731	09:13:42.6	63:07:31.7	0.75	6.0	4.9	—	—	—	1.4	0.67	S
GMRT091343+0632751	09:13:43.5	63:27:51.9	0.46	31.4	23.9	—	12.1	—	5.6	0.77	S
GMRT091346+0644249	09:13:46.5	64:42:49.2	0.96	256.7	162.2	109.0	—	—	37.2	0.89	S
GMRT091347+0632240	09:13:47.0	63:22:40.5	0.53	53.5	37.8	18.0	22.4	—	12.1	0.66	S
GMRT091348+0623508	09:13:48.1	62:35:08.8	1.26	14.2	7.7	—	—	—	4.4	0.50	S
GMRT091349+0641603	09:13:49.9	64:16:03.7	0.55	170.9	111.0	52.0	—	—	17.3	1.09	D
GMRT091352+0625805	09:13:52.1	62:58:05.2	0.89	40.3	25.5	—	—	—	5.8	0.87	S
GMRT091353+0642301	09:13:53.5	64:23:01.2	0.65	117.8	75.5	38.0	—	—	12.1	1.07	S
GMRT091354+0645157	09:13:54.6	64:51:57.8	1.10	10.5	6.2	—	—	—	2.4	0.65	S
GMRT091358+0640801	09:13:58.7	64:08:01.0	0.44	13.2	10.7	—	6.6	—	2.2	0.74	S
GMRT091401+0632103	09:14:01.4	63:21:03.0	0.53	13.6	11.6	—	6.2	—	2.8	0.70	S
GMRT091402+0635652	09:14:02.6	63:56:52.4	0.32	430.2	288.2	183.0	139.4	81.0	57.0	0.85	D
GMRT091402+0651235	09:14:02.7	65:12:35.2	1.43	538.0	236.6	205.0	—	—	65.8	0.99	S
GMRT091403+0625000	09:14:03.9	62:50:00.4	1.01	4.4	3.9	—	—	—	0.7	0.84	S
GMRT091409+0631548	09:14:09.2	63:15:48.8	0.60	5.6	4.9	—	—	—	1.5	0.61	S
GMRT091410+0643332	09:14:10.4	64:33:33.0	0.80	12.2	11.6	—	—	—	3.0	0.66	S
GMRT091415+0640324	09:14:15.0	64:03:24.8	0.36	129.8	100.8	67.0	64.5	—	33.2	0.59	D
GMRT091417+0623840	09:14:17.1	62:38:40.0	1.19	7.5	4.7	—	—	—	3.1	0.37	S
GMRT091424+0640613	09:14:24.1	64:06:13.6	0.39	101.3	91.5	57.0	68.9	—	37.4	0.41	S
GMRT091435+0632643	09:14:35.0	63:26:43.6	0.42	11.9	10.2	—	7.0	—	3.7	0.50	S
GMRT091437+0645522	09:14:37.1	64:55:22.9	1.14	33.7	24.9	16.0	—	—	8.6	0.63	S
GMRT091440+0631316	09:14:40.7	63:13:16.7	0.62	24.2	12.4	—	—	—	3.2	0.90	T
GMRT091445+0641414	09:14:45.3	64:14:14.4	0.48	996.8	756.4	511.0	407.5	—	174.4	0.75	S
GMRT091446+0633757	09:14:46.9	63:37:57.7	0.26	64.2	52.0	—	25.8	—	15.4	0.66	T
GMRT091446+0642706	09:14:46.2	64:27:07.0	0.68	179.1	115.1	56.0	—	—	15.3	1.16	S
GMRT091446+0644244	09:14:46.1	64:42:44.3	0.93	34.5	25.8	20.0	—	—	7.4	0.70	S
GMRT091449+0651507	09:14:49.4	65:15:07.5	1.46	13.3	9.7	—	—	—	5.2	0.41	S
GMRT091452+0622452	09:14:52.2	62:24:52.3	1.40	42.1	18.2	17.0	—	—	4.8	0.96	S
GMRT091508+0633507	09:15:08.2	63:35:07.5	0.27	85.0	60.2	40.0	28.2	—	15.3	0.79	D
GMRT091513+0624944	09:15:13.7	62:49:44.0	0.99	6.4	6.6	—	—	—	6.2	0.02	S
GMRT091515+0651008	09:15:15.4	65:10:08.1	1.37	49.4	24.8	13.0	—	—	8.4	0.82	S
GMRT091518+0650114	09:15:18.3	65:01:14.5	1.23	67.9	46.2	21.0	—	—	11.3	0.85	S
GMRT091520+0630119	09:15:20.4	63:01:19.2	0.79	276.9	175.6	122.0	—	—	34.6	0.95	D
GMRT091520+0632754	09:15:20.7	63:27:54.1	0.36	60.7	46.8	—	18.2	—	7.8	0.93	S
GMRT091520+0635953	09:15:20.3	63:59:53.6	0.24	284.2	178.6	102.0	66.8	34.2	23.1	1.07	D
GMRT091521+0635558	09:15:21.5	63:55:58.1	0.19	11.6	7.3	—	3.4	1.7	—	0.90	S

Table 2 – continued

Source name (1)	RA hh:mm:ss.s (2)	DEC dd:mm:ss.s (3)	Dis deg. (4)	S ₁₅₃ mJy (5)	S ₂₄₄ mJy (6)	S ₃₃₀ mJy (7)	S ₆₁₀ mJy (8)	S ₁₂₆₀ mJy (9)	S ₁₄₀₀ mJy (10)	α (11)	Class (12)
GMRT091523+0624511	09:15:23.8	62:45:11.5	1.06	10.0	5.6	—	—	—	1.2	0.95	S
GMRT091526+0625436	09:15:26.6	62:54:36.7	0.90	16.6	8.8	—	—	—	2.7	0.80	S
GMRT091528+0632939	09:15:28.4	63:29:39.3	0.33	662.4	445.9	337.0	186.9	—	77.5	0.95	S
GMRT091531+0630722	09:15:31.6	63:07:22.0	0.69	9.5	11.0	—	—	—	3.5	0.49	S
GMRT091533+0642008	09:15:33.2	64:20:08.9	0.54	11.8	7.6	—	—	—	4.2	0.44	D
GMRT091540+0650940	09:15:40.7	65:09:40.5	1.36	228.2	123.6	92.0	—	—	35.4	0.86	S
GMRT091543+0625659	09:15:43.8	62:56:60.0	0.86	7.1	3.8	—	—	—	3.3	0.30	S
GMRT091543+0631112	09:15:43.3	63:11:12.8	0.62	6.5	5.7	—	—	—	0.8	0.99	S
GMRT091544+0643404	09:15:44.2	64:34:04.2	0.77	7.5	6.8	—	—	—	2.3	0.55	S
GMRT091544+0645228	09:15:44.3	64:52:28.6	1.08	71.6	43.5	18.0	—	—	5.8	1.19	S
GMRT091549+0634409	09:15:49.8	63:44:09.6	0.11	8.2	2.7	—	1.6	0.5	—	1.21	S
GMRT091550+0631545	09:15:50.3	63:15:45.9	0.55	45.4	29.6	21.0	—	—	8.0	0.79	S
GMRT091552+0635541	09:15:52.3	63:55:41.0	0.15	49.8	32.5	13.0	14.1	5.9	7.5	0.91	T
GMRT091554+0623927	09:15:54.3	62:39:27.0	1.15	6.1	2.9	—	—	—	1.1	0.75	S
GMRT091603+0623034	09:16:03.4	62:30:34.7	1.29	18.1	9.1	—	—	—	2.8	0.82	S
GMRT091612+0641110	09:16:12.1	64:11:10.0	0.39	36.4	28.0	21.0	16.0	—	7.6	0.68	S
GMRT091614+0651445	09:16:14.6	65:14:45.8	1.44	38.6	7.5	—	—	—	3.3	1.07	S
GMRT091616+0623915	09:16:16.7	62:39:15.6	1.15	10.4	7.0	—	—	—	2.7	0.60	S
GMRT091616+0643009	09:16:16.0	64:30:09.5	0.70	5.0	3.6	—	—	—	2.5	0.29	S
GMRT091617+0641327	09:16:17.8	64:13:27.4	0.42	15.1	7.6	—	3.2	—	2.1	0.92	S
GMRT091618+0634929	09:16:18.2	63:49:29.5	0.04	123.1	94.2	—	43.5	20.4	19.5	0.84	S
GMRT091619+0631840	09:16:19.1	63:18:40.5	0.49	76.1	51.4	27.0	24.7	—	14.4	0.77	S
GMRT091621+0622445	09:16:21.8	62:24:45.0	1.39	26.1	15.1	—	—	—	7.1	0.57	S
GMRT091621+0651021	09:16:21.5	65:10:21.5	1.37	28.3	17.3	18.0	—	—	5.6	0.71	S
GMRT091623+0640017	09:16:23.9	64:00:17.4	0.20	7.0	13.6	—	14.5	12.4	9.8	-0.11	S
GMRT091626+0631416	09:16:26.7	63:14:16.4	0.57	159.6	120.3	85.0	—	—	33.1	0.72	D
GMRT091627+0624041	09:16:27.3	62:40:41.4	1.12	12.0	9.2	—	—	—	3.9	0.51	D
GMRT091631+0634820	09:16:32.0	63:48:20.0	0.01	1212.2	826.8	523.0	347.4	—	143.6	0.96	Cplx
GMRT091632+0640438	09:16:32.2	64:04:38.7	0.27	21.1	10.3	—	6.0	2.7	2.5	0.92	S
GMRT091633+0643528	09:16:33.2	64:35:28.1	0.79	263.1	154.6	71.0	—	—	20.6	1.21	D
GMRT091638+0625110	09:16:38.6	62:51:10.5	0.95	7.5	5.2	—	—	—	4.9	0.16	S
GMRT091639+0641738	09:16:39.6	64:17:38.9	0.49	6.0	4.9	—	4.0	—	2.1	0.43	S
GMRT091647+0633008	09:16:47.6	63:30:08.4	0.30	16.9	10.6	—	6.4	1.8	3.3	0.84	S
GMRT091658+0643948	09:16:58.1	64:39:48.4	0.86	147.8	96.0	62.0	—	—	15.9	1.02	S
GMRT091705+0635514	09:17:05.0	63:55:14.7	0.13	12.7	7.2	—	2.5	0.8	—	1.25	S
GMRT091706+0642227	09:17:06.4	64:22:27.7	0.57	24.9	15.4	—	—	—	2.4	1.06	S
GMRT091709+0632430	09:17:09.0	63:24:30.8	0.40	180.7	127.4	90.0	66.9	—	39.4	0.70	D
GMRT091711+0641810	09:17:11.6	64:18:10.8	0.50	4.2	3.3	—	1.1	—	—	0.97	S
GMRT091717+0632106	09:17:18.0	63:21:06.3	0.46	10.7	13.8	—	5.2	—	1.9	0.80	S
GMRT091719+0641734	09:17:19.9	64:17:34.7	0.50	11.2	8.6	—	6.0	—	3.7	0.48	S
GMRT091726+0622734	09:17:27.0	62:27:34.4	1.35	13.7	6.9	—	—	—	2.4	0.76	S
GMRT091728+0633100	09:17:28.5	63:31:00.0	0.30	6.8	5.6	—	2.1	—	—	0.87	S
GMRT091729+0642227	09:17:29.6	64:22:27.5	0.58	62.9	43.2	29.0	—	—	10.9	0.80	D
GMRT091729+0645744	09:17:29.5	64:57:44.3	1.16	22.2	15.5	—	—	—	4.3	0.74	S
GMRT091732+0623932	09:17:32.4	62:39:32.6	1.15	26.2	9.5	—	—	—	4.5	0.75	S
GMRT091733+0650126	09:17:33.4	65:01:26.5	1.23	656.7	354.4	—	—	—	48.1	1.19	S
GMRT091734+0640000	09:17:34.2	64:00:01.0	0.23	98.2	50.2	26.0	13.1	3.1	3.8	1.54	S
GMRT091735+0633739	09:17:35.8	63:37:39.6	0.21	6.1	5.8	—	2.2	0.6	—	1.07	S
GMRT091736+0640522	09:17:36.2	64:05:22.5	0.31	22.8	12.0	—	5.7	2.4	2.2	1.03	S
GMRT091741+0650258	09:17:41.0	65:02:58.5	1.25	472.9	343.0	—	—	—	82.9	0.79	D

Table 2 – continued

Source name (1)	RA hh:mm:ss.s (2)	DEC dd:mm:ss.s (3)	Dis deg. (4)	S ₁₅₃ mJy (5)	S ₂₄₄ mJy (6)	S ₃₃₀ mJy (7)	S ₆₁₀ mJy (8)	S ₁₂₆₀ mJy (9)	S ₁₄₀₀ mJy (10)	α (11)	Class (12)
GMRT091743+0635046	09:17:43.3	63:50:46.8	0.13	3.6	5.5	—	2.3	0.7	—	0.78	S
GMRT091744+0630229	09:17:44.0	63:02:29.5	0.77	20.6	11.5	—	—	—	—	1.1	1.34
GMRT091745+0625955	09:17:45.1	62:59:55.3	0.81	15.5	9.1	—	—	—	—	1.8	0.97
GMRT091748+0622852	09:17:48.5	62:28:52.1	1.33	25.9	16.9	18.0	—	—	—	5.6	0.67
GMRT091749+0631617	09:17:49.5	63:16:17.5	0.55	27.0	19.6	—	—	—	—	3.8	0.89
GMRT091750+0651521	09:17:50.7	65:15:21.0	1.46	274.6	132.2	113.0	—	—	37.5	0.91	D
GMRT091757+0625445	09:17:57.6	62:54:45.2	0.90	153.8	88.7	58.0	—	—	—	11.5	1.18
GMRT091800+0631340	09:18:00.4	63:13:40.0	0.60	27.5	20.4	—	—	—	—	2.1	1.18
GMRT091802+0645918	09:18:02.9	64:59:18.9	1.20	53.1	28.8	—	—	—	—	5.9	0.99
GMRT091803+0634156	09:18:03.1	63:41:56.6	0.19	11.8	11.1	—	5.4	2.0	3.0	0.75	S
GMRT091807+0640831	09:18:07.0	64:08:31.6	0.38	57.3	39.0	—	11.7	—	—	4.1	1.20
GMRT091810+0633919	09:18:10.1	63:39:19.8	0.23	11.8	11.2	—	4.8	—	—	1.7	0.87
GMRT091812+0645112	09:18:12.4	64:51:12.9	1.07	2315.2	1317.2	851.0	—	—	197.6	1.17	D
GMRT091815+0633724	09:18:15.2	63:37:24.9	0.26	33.1	24.2	—	12.5	3.9	7.0	0.83	S
GMRT091827+0641031	09:18:27.2	64:10:31.6	0.43	18.8	22.2	16.0	36.3	—	21.9	-0.17	S
GMRT091841+0635253	09:18:41.2	63:52:53.0	0.24	24.3	21.1	—	11.5	5.6	6.2	0.67	S
GMRT091842+0650229	09:18:42.1	65:02:29.4	1.26	215.8	126.3	117.0	—	—	40.6	0.75	S
GMRT091845+0642854	09:18:45.5	64:28:54.4	0.72	62.4	32.9	17.0	—	—	—	2.5	1.48
GMRT091846+0634654	09:18:46.5	63:46:54.2	0.24	260.5	170.8	112.0	69.2	21.8	30.8	1.05	S
GMRT091847+0625241	09:18:47.5	62:52:41.6	0.96	13.6	13.3	—	—	—	7.7	0.27	S
GMRT091853+0644403	09:18:53.2	64:44:03.8	0.96	24.2	18.6	—	—	—	—	3.3	0.91
GMRT091903+0644834	09:19:03.0	64:48:34.2	1.04	59.2	35.1	21.0	—	—	—	6.2	1.04
GMRT091914+0623359	09:19:14.6	62:33:59.1	1.27	68.1	32.5	—	—	—	—	10.6	0.82
GMRT091914+0634340	09:19:14.2	63:43:40.2	0.30	6.5	3.9	—	1.9	—	—	0.87	S
GMRT091929+0641436	09:19:29.4	64:14:36.0	0.54	16.3	14.8	—	—	—	—	3.1	0.77
GMRT091930+0642537	09:19:30.3	64:25:37.4	0.70	175.7	123.7	89.0	—	—	32.8	0.77	S
GMRT091938+0622856	09:19:38.9	62:28:56.3	1.36	30.8	19.4	14.0	—	—	—	8.2	0.60
GMRT091946+0640544	09:19:46.8	64:05:44.7	0.46	14.5	8.1	—	4.5	—	—	2.1	0.84
GMRT091947+0650953	09:19:47.1	65:09:53.5	1.40	250.1	143.5	118.0	—	—	—	42.1	0.81
GMRT091948+0625832	09:19:48.6	62:58:32.8	0.90	1643.9	1062.9	788.0	—	—	241.0	0.89	D
GMRT091957+0643231	09:19:57.4	64:32:31.5	0.83	124.5	75.9	38.0	—	—	—	11.6	1.11
GMRT091957+0643800	09:19:57.9	64:38:00.2	0.91	25.8	17.6	—	—	—	—	9.2	0.45
GMRT092002+0631414	09:20:02.3	63:14:14.2	0.68	202.1	131.5	83.0	—	—	—	24.6	0.97
GMRT092002+0634606	09:20:02.6	63:46:06.7	0.38	22.1	19.3	—	8.5	—	—	5.2	0.69
GMRT092004+0633626	09:20:04.4	63:36:26.5	0.43	22.5	8.6	—	2.9	—	—	—	1.49
GMRT092009+0641550	09:20:09.6	64:15:50.1	0.60	256.5	145.9	94.0	—	—	—	14.4	1.30
GMRT092016+0632357	09:20:16.1	63:23:57.1	0.57	19.0	14.0	—	—	—	—	3.3	0.79
GMRT092020+0644259	09:20:20.5	64:42:59.5	1.00	31.5	21.4	—	—	—	—	3.9	0.95
GMRT092022+0630258	09:20:22.9	63:02:58.0	0.86	13.0	11.0	—	—	—	—	3.6	0.59
GMRT092022+0635143	09:20:22.5	63:51:43.6	0.42	93.9	66.7	36.0	31.1	—	—	15.7	0.82
GMRT092025+0624607	09:20:25.7	62:46:07.3	1.12	36.9	21.3	16.0	—	—	—	5.4	0.87
GMRT092030+0635437	09:20:30.4	63:54:37.3	0.44	5.9	3.1	—	1.4	—	—	—	1.05
GMRT092033+0633921	09:20:34.0	63:39:21.8	0.46	10.5	8.2	—	3.4	—	—	2.6	0.69
GMRT092033+0650452	09:20:33.4	65:04:52.6	1.35	27.9	20.3	—	—	—	—	6.1	0.69
GMRT092034+0643829	09:20:35.0	64:38:29.9	0.94	61.4	41.1	19.0	—	—	—	9.8	0.87
GMRT092036+0630453	09:20:36.0	63:04:53.7	0.85	15.7	10.4	—	—	—	—	4.5	0.55
GMRT092040+0623255	09:20:40.3	62:32:55.8	1.34	13.8	12.0	—	—	—	—	6.0	0.38
GMRT092045+0630309	09:20:45.9	63:03:09.3	0.88	23.2	18.9	14.0	—	—	—	6.0	0.62
GMRT092056+0640008	09:20:57.0	64:00:08.2	0.52	13.8	11.2	—	4.0	—	—	—	0.91
GMRT092057+0632047	09:20:57.1	63:20:47.3	0.67	8.1	12.9	—	—	—	—	6.7	0.16

Table 2 – continued

Source name (1)	RA hh:mm:ss.s (2)	DEC dd:mm:ss.s (3)	Dis deg. (4)	S ₁₅₃ mJy (5)	S ₂₄₄ mJy (6)	S ₃₃₀ mJy (7)	S ₆₁₀ mJy (8)	S ₁₂₆₀ mJy (9)	S ₁₄₀₀ mJy (10)	α (11)	Class (12)
GMRT092106+0623042	09:21:06.8	62:30:42.9	1.39	55.4	28.5	25.0	—	—	11.1	0.72	S
GMRT092111+0641445	09:21:11.3	64:14:45.6	0.67	69.8	41.5	—	—	—	12.4	0.77	S
GMRT092118+0645237	09:21:18.3	64:52:37.2	1.19	958.3	599.3	452.0	—	—	134.9	0.90	S
GMRT092123+0643404	09:21:23.6	64:34:04.4	0.93	100.5	79.4	31.0	—	—	52.1	0.32	Cplx
GMRT092131+0633939	09:21:31.9	63:39:39.6	0.57	114.2	60.5	40.0	—	—	4.0	1.50	D
GMRT092138+0623054	09:21:38.4	62:30:54.9	1.41	151.3	76.1	77.0	—	—	32.2	0.69	S
GMRT092143+0641520	09:21:43.6	64:15:20.8	0.72	320.9	184.0	141.0	—	—	60.6	0.77	Cplx
GMRT092145+0623528	09:21:45.1	62:35:28.8	1.34	163.6	83.3	83.0	—	—	22.2	0.88	S
GMRT092149+0640311	09:21:49.5	64:03:11.3	0.63	36.5	25.1	—	—	—	6.3	0.79	D
GMRT092150+0634702	09:21:50.9	63:47:02.0	0.58	56.9	47.2	27.0	—	—	11.0	0.77	S
GMRT092209+0651030	09:22:09.7	65:10:30.5	1.50	474.2	193.0	168.0	—	—	32.4	1.24	S
GMRT092219+0633655	09:22:19.5	63:36:55.4	0.66	3351.8	2174.2	1486.0	—	—	310.7	1.05	S
GMRT092219+0650556	09:22:20.0	65:05:56.4	1.44	232.8	98.7	93.0	—	—	17.9	1.15	D
GMRT092228+0623756	09:22:28.3	62:37:56.4	1.35	12.1	7.7	—	—	—	2.1	0.78	S
GMRT092234+0625237	09:22:34.1	62:52:37.0	1.14	58.4	35.6	17.0	—	—	11.9	0.75	S
GMRT092234+0640556	09:22:34.7	64:05:56.9	0.72	201.0	119.8	80.0	—	—	37.7	0.78	T
GMRT092235+0623518	09:22:35.3	62:35:18.9	1.39	15.2	7.4	—	—	—	2.0	0.89	S
GMRT092251+0630618	09:22:51.7	63:06:18.9	0.99	59.5	39.1	22.0	—	—	8.1	0.93	S
GMRT092255+0645259	09:22:55.1	64:52:59.7	1.28	112.6	54.5	39.0	—	—	12.0	1.03	S
GMRT092302+0632925	09:23:02.9	63:29:25.0	0.78	38.5	29.1	39.0	—	—	23.4	0.20	S
GMRT092307+0632853	09:23:07.4	63:28:53.0	0.79	16.6	17.7	—	—	—	23.4	-0.16	S
GMRT092309+0623246	09:23:09.2	62:32:46.9	1.46	9.1	6.6	—	—	—	3.6	0.41	S
GMRT092311+0632429	09:23:11.7	63:24:29.2	0.83	31.9	18.8	—	—	—	5.4	0.79	S
GMRT092312+0633140	09:23:12.1	63:31:40.5	0.78	158.7	94.3	72.0	—	—	17.5	1.00	D
GMRT092318+0643531	09:23:18.0	64:35:31.3	1.08	30.2	11.7	—	—	—	5.6	0.72	D
GMRT092323+0630847	09:23:23.9	63:08:47.0	1.00	91.2	56.4	39.0	—	—	14.3	0.85	S
GMRT092324+0630643	09:23:24.9	63:06:43.5	1.03	133.8	74.1	51.0	—	—	14.2	1.03	D
GMRT092332+0632817	09:23:32.8	63:28:17.2	0.84	760.3	461.8	319.0	—	—	81.0	1.03	T
GMRT092332+0633611	09:23:32.4	63:36:11.9	0.80	89.0	48.6	38.0	—	—	4.6	1.31	Cplx
GMRT092344+0641122	09:23:44.1	64:11:22.3	0.87	8.5	5.0	—	—	—	1.2	0.86	S
GMRT092355+0625336	09:23:55.2	62:53:36.4	1.23	1130.4	785.9	763.0	—	—	299.6	0.58	S
GMRT092401+0645058	09:24:01.3	64:50:58.5	1.32	275.7	141.8	119.0	—	—	37.3	0.91	D
GMRT092401+0645641	09:24:01.7	64:56:41.4	1.40	16.2	11.4	—	—	—	3.2	0.73	S
GMRT092403+0623912	09:24:03.4	62:39:12.6	1.42	59.1	33.9	19.0	—	—	10.2	0.82	D
GMRT092408+0641424	09:24:08.9	64:14:24.8	0.94	15.8	21.8	16.0	—	—	15.2	0.06	S
GMRT092412+0632324	09:24:12.4	63:23:24.2	0.94	25.8	9.7	—	—	—	2.8	0.98	S
GMRT092412+0643911	09:24:12.8	64:39:11.4	1.19	9.2	8.4	—	—	—	2.9	0.54	S
GMRT092412+0645922	09:24:12.3	64:59:22.7	1.44	12.8	6.3	—	—	—	3.1	0.60	S
GMRT092428+0632912	09:24:28.6	63:29:12.7	0.93	11.1	7.7	—	—	—	4.3	0.41	S
GMRT092428+0635917	09:24:28.6	63:59:18.0	0.89	48.0	16.6	—	—	—	3.2	1.21	D
GMRT092434+0635751	09:24:34.8	63:57:51.0	0.89	16.1	11.4	—	—	—	1.5	1.08	S
GMRT092441+0634926	09:24:41.8	63:49:26.6	0.89	21.7	12.8	—	—	—	4.6	0.69	S
GMRT092459+0643337	09:24:59.4	64:33:37.5	1.19	46.1	22.3	18.0	—	—	8.5	0.76	S
GMRT092501+0635941	09:25:01.8	63:59:41.6	0.95	21.8	13.7	—	—	—	3.9	0.77	S
GMRT092526+0632708	09:25:26.4	63:27:08.6	1.04	122.9	74.9	47.0	—	—	21.3	0.82	S
GMRT092530+0640832	09:25:30.2	64:08:33.0	1.04	9.7	14.5	—	—	—	4.6	0.41	S
GMRT092540+0644841	09:25:40.3	64:48:41.0	1.41	41.4	16.0	—	—	—	5.0	0.93	S
GMRT092549+0631414	09:25:49.5	63:14:14.4	1.17	106.5	63.8	56.0	—	—	15.2	0.87	D
GMRT092551+0645158	09:25:51.6	64:51:58.7	1.46	53.8	26.5	33.0	—	—	5.5	0.98	S
GMRT092608+0632559	09:26:08.7	63:25:59.6	1.12	122.2	75.1	37.0	—	—	15.9	0.97	S

Table 2 – continued

Source name (1)	RA hh:mm:ss.s (2)	DEC dd:mm:ss.s (3)	Dis deg. (4)	S ₁₅₃ mJy (5)	S ₂₄₄ mJy (6)	S ₃₃₀ mJy (7)	S ₆₁₀ mJy (8)	S ₁₂₆₀ mJy (9)	S ₁₄₀₀ mJy (10)	α (11)	Class (12)
GMRT092635+0633938	09:26:35.4	63:39:38.8	1.12	34.1	19.2	—	—	—	4.0	0.96	S
GMRT092639+0632523	09:26:39.2	63:25:23.0	1.18	28.3	15.8	—	—	—	4.3	0.84	S
GMRT092643+0635212	09:26:43.3	63:52:12.7	1.12	64.0	40.1	25.0	—	—	12.3	0.76	S
GMRT092647+0631454	09:26:47.7	63:14:54.5	1.27	46.2	22.5	—	—	—	6.8	0.85	S
GMRT092652+0641938	09:26:52.4	64:19:38.0	1.24	4665.0	3030.9	2606.0	—	—	1093.4	0.74	S
GMRT092655+0633256	09:26:55.3	63:32:56.6	1.17	211.7	122.7	97.0	—	—	33.6	0.84	T
GMRT092701+0643748	09:27:01.0	64:37:48.8	1.40	402.6	161.6	148.0	—	—	34.1	1.14	D
GMRT092718+0635018	09:27:18.3	63:50:18.8	1.18	32.2	15.5	—	—	—	2.7	1.11	D
GMRT092756+0634755	09:27:56.8	63:47:55.9	1.25	87.0	66.3	46.0	—	—	30.5	0.49	S
GMRT092809+0635356	09:28:09.7	63:53:56.5	1.28	371.8	179.3	127.0	—	—	38.5	1.07	D
GMRT092819+0632001	09:28:19.7	63:20:01.3	1.39	40.6	19.2	20.0	—	—	8.8	0.66	D
GMRT092830+0634748	09:28:30.7	63:47:48.8	1.32	96.8	33.1	23.0	—	—	—	1.95	E
GMRT092830+0641530	09:28:30.7	64:15:30.2	1.38	37.4	21.9	—	—	—	9.7	0.59	D
GMRT092857+0635912	09:28:57.0	63:59:12.9	1.37	190.3	80.5	60.0	—	—	21.1	1.02	D
GMRT092858+0634653	09:28:58.4	63:46:53.5	1.37	59.6	27.5	28.0	—	—	8.5	0.86	S
GMRT092915+0633058	09:29:15.2	63:30:59.0	1.43	95.8	42.3	28.0	—	—	11.6	0.98	S
GMRT092930+0635029	09:29:30.9	63:50:29.3	1.43	95.7	43.6	34.0	—	—	11.2	0.98	S